DOE/ET-53088-362 IFSR #362

The Dynamics of Ion Rings in Highly Conductive Plasmas

P.M. Lyster and *R.N. Sudan* *
Institute for Fusion Studies
The University of Texas at Austin
Austin, Texas 78712

**Laboratory of Plasma Studies, Cornell University*

January 1989

The Dynamics of Ion Rings in Highly Conductive Plasmas

P.M. Lyster and R.N. Sudan*
Institute for Fusion Studies
University of Texas at Austin
Austin, Texas 78712

Abstract

A numerical study is made of the dynamics of translating ion rings in conductive plasmas. A hybrid computer code (particle ions/fluid electrons) is employed. An important process whereby translational kinetic energy of such rings may be removed is via the generation of Alfvén waves. When the initial axial velocity of the ring is greater than the local Alfvén speed in the plasma, a typical slowing down length is $z_A \approx (a_r/4\zeta)v_{z0}^4/(v_\theta^2 v_A^2)$ where a_r is the ring radial width, $\zeta = \delta B/B_0$ where δB is an estimate of the ring self magnetic field strength, and B_0 is the strength of the axial magnetic field, v_{z0} is the initial translational velocity of the ring, v_θ is the average toroidal ring particle velocity and $v_A = B_0/\sqrt{4\pi\rho}$ is the Alfvén velocity, where ρ is the plasma mass density. Also discussed is the dynamics of ion ring motion in the vicinity of a field reversed configuration.

(submitted to Phys. Fluids)

*Laboratory of Plasma Studies, Cornell University, Ithaca, New York 14853

I. Introduction

Previous studies have shown that closed magnetic field line ion rings may be useful for confining plasmas for magnetic fusion.[1,2] Ion rings may also provide a part of the current of a field reversed configuration (FRC) for the purpose of for heating the confined plasma or stabilizing it against macroscopic instabilities.[3] For the latter situation, ion rings may be formed and then merged with the FRC. However, if there is any excess translational energy in the ring formation, this could be deleterious to the merging process. This excess energy may be removed by the resistive dissipation of plasma return currents that are generated due to the motion of the ring.[7] Alternatively, it may be accomplished by the generation of Alfvén waves in a conductive plasma, and this is the process that we are mainly concerned with in this paper.

The usual configuration for translating ion rings is shown in Figure 1. The figure shows the r, z plane of a cylinder, where the ring of N_b ions is translating axially (z) in an external magnetic field $\boldsymbol{B}_0 = (B_{z0} B_{\theta 0})$. Generally, the theta magnetic field is either absent or smaller than the axial field. The axial velocity v_z is usually small compared with typical ion velocities in the theta direction, such that the ratio of translational to total kinetic energies is $K_z/K \approx 0.1$. The axial and radial widths are a_z and a_r, respectively. In the present numerical study, the rings are assumed to be not excessively elongated, that is $a_z/a_r \sim 0(2)$. Immersed in the magnetic field is a background plasma of density n_p and conductivity σ.

Molvig and Rostoker[8] give a physical description of the process of wave generation in terms of the Chernkov resonance condition $\omega(k_\perp, k_z) = k_z v_z$, where $k_\perp \approx 2\pi/a_r$ and $k_z \approx 2\pi/a_z$. For a cold plasma, in the limit $|k|c/\omega_i \ll 1$ and $\omega < \Omega_{LH}, \Omega_i$, the magnetosonic wave has dispersion relation $\omega = |k| v_A$ where $k^2 = k_\perp^2 + k_z^2$. The branch that is perpendicular to the magnetic field has a resonance at the lower hybrid frequency Ω_{LH}, while in the parallel direction it becomes the whistler branch when $k_z c/\omega_i > 1$. Another candidate is the shear

Alfvén wave which has a dispersion relation $\omega = k_z v_A$; this wave travels along the field lines, parallel with the translating ring. In experimental situations where the wave velocity is less than v_z, there can be no resonance for the shear wave. However, the magnetosonic wave can travel perpendicular to the field lines, thus satisfying the Cherenkov condition. In the limit that $v_z \gg v_A$, the ring generates a magnetosonic wave which travels radially outward to the wall.

Chu and Rostoker[9] recognized that the axial slowing down of the ring particles is via the Lorentz $v_{b_\theta} \delta B_r / c$ force. The magnetic field lines move out radially with the plasma ions, and this generates a radial magnetic field δB_r. Molvig and Rostoker[8] calculated a slowing down length based on the two fluid model with non-self consistent beam dynamics. However, they did this for a critically damped magnetosonic wave ($\nu^e = 2(\Omega_e \Omega_i)^{1/2} = 2\Omega_{LH}$), where ν^e is the electron collision frequency, and Ω_e and Ω_i are the electron and ion cyclotron frequencies, respectively. This calculation then gave rise to resistive slowing down lengths, these have also been studied by the present authors in a related paper.[7]

This slowing down length for relativistic electrons is

$$z_\sigma = \frac{1}{2} \frac{n_p}{n_b} \left(\frac{v_z}{c} \right)^3 \frac{\gamma}{\kappa} \frac{c}{\nu^e}$$

n_b is now the beam ion number density $\gamma = 1/v(1 - v^2/c^2)$, and $\kappa = 1 + \Omega_e \Omega_i / \nu^e \nu^i$. This corresponds to Eq. (13b) in Ref. 7 in the non-relativistic case considered by Lyster and Sudan.[7] In another paper Molvig and Rostoker[10] calculate, in slab geometry, the kinetic energy transferred between a layer and the magnetosonic waves. Their model assumes axial invariance $\partial_z = 0$, and the energy removed from the layer is that which is transferred to the self-magnetic field energy. In open slab geometry, with the assumption of non-self-consistent layer dynamics, there is no limit to the energy which is transferred to the magnetosonic wave. In one dimensional cylindrical geometry, Peter and Rostoker[11] showed that the maximum energy per unit length which is transferred is $W = (2\pi R_b I_0 / c)^2 (1 - R_b^2 / R_w^2)$, where I_0 is

the layer current per unit length. The energy is limited by the localization of the layer self-magnetic fields. For a ring of finite length this energy is approximately νK_0 where $\nu = N_b r_{ci}/R_b$, $r_{ci} = e^2/m_i c^2$ and K_0 is the theta ring kinetic energy. In the above analyses no attempt was made to use the generation of plasma waves to calculate the axial dynamics of the ring.

Alfvén wave activity has been observed in some ring translation experiments. Roberson[12,13] showed that the above equation gives a reasonable estimate for the observed axial slowing down of electron rings in a resistive plasma. Also for preionized plasma, magnetic field fluctuations characteristic of the magnetosonic mode were observed. Similar observations were made by Kapetanakos et al.[14] for rotating relativistic electron rings, and Golden et al.[15] and Schamiloglu[13] for translating ion rings.

Some experiments in which electron rings were trapped involved using an external theta magnetic field. This field was imposed by passing a current through a conductor on axis. This has been found necessary in the case of vacuum stacking of layers in the Astron experiment to avoid particle losses due to the electrostatic precessional instability.[16,17,18] For some high plasma density runs on the Astron experiment, there was observed an unusual enhancement in the electron layer trapping efficiency with this external field present.[19] Also, for ring stacking work done at Cornell's Relativistic-Electron-Coil-Christa experiment (RECE), it was found that the theta field enhanced the ability to trap the rings.[20] The theta magnetic field had to be in excess of that needed to stabilize the magnetic precessional instability in order to trap the rings.[21] Although the above experiments were carried out in a resistive plasma, the question can be asked: what effect will the theta magnetic field have on the Alfvén wave slowing down mechanism?

Once a ring has slowed down to $v_z < v_A$, the self-magnetic field associated with the toroidal current are formed. The generation of Alfvén waves ($v_z > v_A$) and self-fields ($v_z < v_A$) may be thought of as radiative and non-radiative limits respectively. In some

experimental situations it may be necessary to translate a ring along with its self-fields toward an FRC. The collective interaction between the particles and self-fields have already been discussed in a previous paper relating to dynamics in resistive plasmas,[1] and the results of simulation for a conductive plasma will be discussed here. Where the self-fields (δB) are so strong that the moving ring becomes field reversed ($\zeta = |\delta B/B_0| = 1$), highly nonlinear phenomena, in particular, magnetic field line reconnection, may become important. This will be discussed in a future paper.

In the following section the theoretical description of ion ring dynamics in axisymmetric ($\partial_\theta = 0$) geometry is presented. Firstly, we discuss single particle motion that is relevant for the case of weak ion rings ($\zeta \ll 1$), and then the collective ion ring motion is analyzed. In section III the result of particle code simulations is presented. The main results are for the case $v_z > v_A$ with only an axial (B_z) field present. Some simulations were performed to check the single particle and collective ring motion in the presence of both B_θ and B_z, and a discussion is made for the case of slowing down when $v_z < v_A$. Finally, some simulations are presented for the behavior of rings which have weak but finite field reversal factors ζ in the presence of an FRC.

II. Theoretical Description of the Translation of Ion Rings

A. Single Particle Dynamics

Consider first the case where the self-field of the ring $\delta\boldsymbol{B}$ is much weaker than $\boldsymbol{B}_0$. The particle motion is unperturbed by $\delta\boldsymbol{B}$ and the ring can be fully described as a set of single particle orbits. Assuming that there are no electrostatic fields present, the motion is described by the Lorentz force law

$$m\frac{d}{dt}\boldsymbol{v} = \frac{q}{c}\boldsymbol{v} \times \boldsymbol{B}_0$$

where $\boldsymbol{v} = v_r\hat{r} + v_\theta\hat{\theta} + v_z\hat{z}$ is the velocity, q is the charge, and m is the mass. It is well known[22] that in asymmetric geometry ($\partial_\theta = 0$) each particle has a constant of the motion; the cannonical angular momentum

$$P_\theta = mrv_\theta + \frac{e}{c}\psi \tag{1}$$

and a potential energy function

$$H^* = \frac{1}{2mr}\left(P_\theta - \frac{e}{c}\psi\right)^2 \tag{2}$$

such that the poloidal (r, z) motion is described by the equation

$$m(\dot{v}_r\hat{r} + \dot{v}_z\hat{z}) = -\nabla H^* + \frac{q}{c}\boldsymbol{v}_\rho \times \boldsymbol{B}_\theta \tag{3}$$

where $\boldsymbol{B}_\rho = \nabla\psi \times \hat{\theta}/r$ is the poloidal magnetic field and $\boldsymbol{v}_\rho = v_r\hat{r} + v_\theta\hat{\theta}$. Taking the dot product of $\boldsymbol{v}_\rho$ with Eq. (3) gives

$$\frac{d}{dt}(\frac{1}{2}mv_\rho^2 + H^*) = 0 \tag{4}$$

where $d/dt \equiv \partial/\partial t + \mathrm{v}_\rho \cdot \nabla$. Equation (4) described the interaction between the poloidal kinetic and the potential energies; the poloidal motion is confined by contours of H^*. Note that the result is independent of the toroidal magnetic field structure.

Consider a particle injected in a uniform axial field $B_z > 0$ (axial variations are ignored), at radius r_b, with axial velocity v_{z0}, and theta velocity $v_\theta = -r_b\Omega_z$, where $\Omega_z = eB_z/mc$. Then

$$H^* = \frac{m}{8}\Omega_z^2\frac{(r_b^2 + r^2)}{r^2}. \tag{5}$$

Thus $\nabla H^* = 0$ at $r = r_b$, and the poloidal force is determined by the second term in Eq. (3). Of interest here is the poloidal motion of the particle as parameterized by the quantities B_θ/B_z and $f = (v_{z0}/v_\theta)^2$. When f is small and B_θ/B_z is large, the poloidal Larmor radius

of the particle will be small compared with the scale length of magnetic field variations. Therefore, the drift approximation will apply, and the expression for the drift velocity[23] is

$$\boldsymbol{v}_d = \frac{c}{e}\frac{\langle \boldsymbol{F} \rangle \times \boldsymbol{B}_\theta}{B_\theta^2} \tag{6}$$

where $\langle \boldsymbol{F} \rangle$ is the orbit averaged force on the particle. Since there are no axial variations in the field, only the radius r of the particle is important in calculating $\langle \boldsymbol{F} \rangle$. Write $r = r_b + r_{i\theta} S(1+\sin\Omega_\theta t)$, where $S = -\text{sign}(B_\theta)$, $B_\theta = B_{\theta 0} r_w / r$, $B_{\theta b} = B_\theta(r = r_b)$, $\Omega_\theta = eB_{\theta b}/mc$ and $r_{i\theta} = v_{z0}/\Omega_\theta$. Then the force corresponding to the first term in Eq. (3) is

$$\langle \boldsymbol{F} \rangle_H = \frac{\Omega_\theta}{2\pi}\int_0^{\frac{2\pi}{\Omega_\theta}} dt(-\nabla H^*) = \left(Sm\Omega_z^2 r_{i\theta} + O\left(\frac{r_{i\theta}}{r_b}\right)^2 \right)\hat{z}. \tag{7}$$

The drift velocity corresponding to this force is

$$\boldsymbol{v}_H = v_{z0}\left(B_z/B_{\theta b}\right)^2 \hat{z}, \tag{8}$$

and this is always in the direction of the axial injection velocity.

The second term in Eq. (3) gives rise to a gradient drift due to the $1/r$ dependence in the toroidal magnetic field. The expression for the gradient drift velocity is

$$\boldsymbol{v}_{\nabla B} = \frac{e}{c}\mu_\perp \frac{\boldsymbol{B}_\theta \times \nabla B_\theta}{B_\theta^2} \tag{9}$$

where the magnetic moment is $\mu_\perp = mv_{z0}^2/2|B_{\theta b}|$. In the geometry described above, this is evaluated to be

$$\mathrm{v}_{\nabla B} = \frac{1}{2}\sqrt{f} v_{z0}\frac{B_z}{B_{\theta b}}\hat{z}. \tag{10}$$

The drift direction depends on the sign of the theta magnetic field. The net drift in the z direction is

$$\mathrm{v}_D = \mathrm{v}_{\nabla B} + \mathrm{v}_H = v_{z0}\left(\frac{1}{2}\sqrt{f}\frac{B_z}{B_{\theta b}}\right) + \left(\frac{B_z}{B_{\theta b}}\right)^2 \hat{z}. \tag{11}$$

For a fixed value of f, the behavior of the drifts is divided into a number of regimes. The following lists the values of $B_{\theta b}$ which delineate these regimes:

(1) $|B_{\theta b}/B_z| \gg 1; v_D = v_{\nabla b}$.

(2) $B_{\theta 1}/B_z = -\left(4/\sqrt{f}\right)$; at this value of toroidal magnetic field, the net drift velocity in the negative z direction, Eq. (9) is maximized. This velocity is $(v_D/v_{z0}) = -f/16$.

(3) $B_{\theta_2}/B_z = -\left(2/\sqrt{f}\right)$; at this point the drift velocities cancel, $\mathrm{v}_d = 0$, and the particle remains at a fixed axial position while performing a small Larmor radius orbit in the poloidal plane.

(4) $B_{\theta_3}/B_z = -\sqrt{f}/\left(\sqrt{(f+1)} + \sqrt{f} - 1\right)$; here the particle performs cusp-like motion as it drifts in the positive z direction. This expression is obtained by equating the approximate expression for the poloidal Larmor radius $v_{z0}/\Omega_{i\theta}$, with $R_{\max} - r_b$, where $R_{\max} = \left(\sqrt{(f+1)} + \sqrt{f}\right) r_b$ is the maximum radius which is energetically accessible to the particle. Therefore, $B_{\theta 3}$ is the approximate magnetic field at which the particle motion changes over from being a cyclotron orbit in the poloidal plane to a wavy drift in the axial direction.

(5) $B_{\theta b} = 0$; Eq. (9) is inaccurate since the particle does not perform small Larmor radius orbits in the poloidal plane. In fact, when the theta magnetic field is zero, the average axial drift velocity, $\langle v_z \rangle$ is trivially equal to the initial injection velocity v_{z0}.

(6) $B_{\theta_4}/B_z = \sqrt{f}/\left(1 - \sqrt{(f+1)} + \sqrt{f}\right)$; for this positive value of the theta magnetic field, the particle performs cusp-like motion in the poloidal plane. However, unlike the particle in category (4) above, the cusp is determine by the particle reaching the minimum accessible radius, $r_{\min} = \left(\sqrt{(f+1)} - \sqrt{f}\right) r_b$.

For a fixed value of the ratio of poloidal to toroidal injection energy, $f = 0.2$, the corresponding values of the relevant important ratios, as set out above, are: $B_{\theta 1}/B_z = -8.94$ (with $(v_D/v_{z0})_{\min} = -0.012$), $B_{\theta 2}/B_z = -4.47$, $B_{\theta 3}/B_z = -0.83$, and $B_{\theta 4}/B_z = 1.27$.

B. Ion Ring Excitation of Alfvén Waves

Consider an ion ring that is translating axially in a conductive plasma in an external solenoidal field B_0. The energetic ring ions will be considered to be collisionless. For the plasma, the two fluid equations are employed,[24] and an analytical reduction is performed in the manner of Sudan and Lyster.[25] The equations for the plasma ion mass density ρ_i and fluid velocity $\mathbf{v}_i$ are

$$\partial_t \rho_i + \nabla \cdot \rho_i \mathbf{v}_i = 0, \tag{12}$$

$$\rho_i \frac{d}{idt} \mathbf{v}_i = -n_b Z_b e \boldsymbol{E} + \boldsymbol{J}_p \times \boldsymbol{B}/c, \tag{13}$$

where the plasma current $\boldsymbol{J}_p = (n_i z_i \boldsymbol{v}_i - n_e e \boldsymbol{v}_e) \sim n_e e(\mathbf{v}_i - \mathbf{v}_e)$; the plasma is quasineutral $n_e = Z_i n_i + Z_b n_b$ and $n_b \ll n_i$; and the subscripts b, i and e refer to ring ions, plasma ions and electrons respectively. The inertial term in the electron fluid momentum equation is neglected. Combining this equation with Faraday's law gives

$$\partial_t \boldsymbol{B} = \nabla \times \mathbf{v}_e \times \boldsymbol{B} - c \nabla \times \mathbf{J}_p/\sigma. \tag{14}$$

Finally, Ampere's law without the displacement current is

$$\frac{c}{4\pi} \nabla \times B = \boldsymbol{J}_p + \boldsymbol{J}_b. \tag{15}$$

For a cold plasma, the pressure term $\nabla(P_e + P_i)$ has been neglected in the moment equation (13). For ring injection studies, the electron $\mathbf{E} \times \mathbf{B}$ drift motion is responsible for the return current. Thus, the first term in Eq. (13) is approximately $-(n_b/n_p) Z_b \mathbf{J}_p \times \mathbf{B}/c$, which may be neglected relative to the second term to order $n_b/n_p \ll 1$. Next, use Eq. (15) to eliminate $\mathbf{v}_e$ and $\mathbf{J}_p$ from Eqs. (13) and (14) in favor of $\mathbf{v}_i$, $\mathbf{J}_b$ and $\nabla \times \mathbf{B}$

$$\rho \frac{d}{dt} \mathbf{v} = (\nabla \times \mathbf{B}) \times \mathbf{B}/4\pi - \mathbf{J}_b \times \mathbf{B}/c, \tag{16}$$

$$\begin{aligned} \partial_t \mathbf{B} &= \nabla \times \mathbf{v} \times \mathbf{B} - \nabla \times \left(\frac{1}{ne} \left(\frac{c}{4\pi} \nabla \times \mathbf{B} - \mathbf{J}_b \right) \times \mathbf{B} \right) \\ &\quad - \frac{c^2}{4\pi\sigma} \nabla \times \nabla \times \mathbf{B} + \frac{c}{\sigma} \nabla \times \boldsymbol{J}_b, \end{aligned} \tag{17}$$

where the subscripts have been dropped from ρ_i, $\mathbf{v}_i$ and n_i. Now write $\mathbf{B} = \mathbf{B}_\rho + B_\theta\hat{\theta}$, invoke axisymmetry, and neglect the poloidal components of the ring current; Eqs. (16) and (17) can be rewritten in the form[25]

$$\partial_t\psi + \mathbf{v}\cdot\nabla\psi = \frac{c^2}{4\pi\sigma}\Delta_*\psi + \frac{cr}{\sigma}J_{b\theta} - \frac{c}{4\pi ne}\mathbf{B}_\rho\cdot\nabla rB_\theta, \tag{18}$$

$$\begin{aligned}\partial_t B_\theta + \mathbf{v}\cdot\nabla B_\theta &= -B_\theta\nabla\cdot\mathbf{v} + B_\theta v_r/r + rB_\rho\cdot\nabla\frac{v_\theta}{r} + r\mathbf{B}_\rho\cdot\nabla\frac{1}{ner}\left(J_b + \frac{c}{4\pi r}\Delta_*\psi\right)\\ &\quad + \frac{c}{4\pi}\hat{\theta}\cdot\nabla\left(\frac{1}{ner^2}\right)\times\nabla r^2B_\theta^2/2 + \frac{c^2}{4\pi\sigma}(\nabla^2B_\theta - B_\theta/r^2),\end{aligned} \tag{19}$$

$$\rho\left(\partial_t\mathbf{v}_\rho + \mathbf{v}_\rho\cdot\nabla v_\rho - \frac{v_\theta^2\hat{r}}{r}\right) = -\left(\frac{1}{4\pi r^2}\Delta_*\psi + \frac{1}{cr}J_b\right)\nabla\psi - \frac{1}{r^2}\nabla\frac{r^2B_\theta^2}{8\pi}, \tag{20}$$

$$\rho\left(\partial_t v_\theta + \mathbf{v}_\rho\cdot\nabla v_\theta + \frac{v_\theta v_r}{r}\right) = \frac{1}{4\pi r}\mathbf{B}_\rho\cdot\nabla rB_\theta \tag{21}$$

where $\mathbf{v} = \mathbf{v}_\rho + v_\theta\hat{\theta}$ and $\Delta_* = \nabla^2 - 2\partial/r\partial r$.

The rate of change of kinetic energy K of the injected ring is given by

$$\begin{aligned}\frac{d}{dt}K \equiv \frac{d}{dt}\sum_k\frac{1}{2}m_bv_k^2 &= \int d^3x\mathbf{J}_b\cdot\mathbf{E} = \int d^3x\,(J_{b_\theta}E_\theta)\\ &= -\frac{2\pi}{c}\int rdrdzJ_{b_\theta}\partial_t\psi,\end{aligned} \tag{22}$$

where k is a ring particle subscript. The neglect of the term $J_{bz}E_z$ can be justified on the grounds that $|J_{bz}| \ll |J_{b\theta}|$. From Eqs. (18) to (21) the equations for the perturbed field and fluid quantities are

$$\begin{aligned}\partial_t\delta\psi &= -\delta\mathbf{v}_\rho\cdot\nabla\psi_0 - \frac{c}{4\pi n_0e}\mathbf{B}_{\rho_0}\cdot\nabla r\delta B_\theta + \frac{cr}{\sigma}J_{b_\theta}\\ &\quad + \frac{c^2}{4\pi\sigma}\Delta_*\delta\psi,\end{aligned} \tag{23}$$

$$\partial_t\delta B_\theta = r\mathbf{B}_{\rho_0}\cdot\nabla\left(\left(J_{b_\theta} + \frac{c}{4\pi r}\nabla_*\delta\psi\right)/n_0er + \delta v_\theta/r\right), \tag{24}$$

$$\rho_0\partial_t\delta v_r = -\frac{J_{b_\theta}}{cr}\nabla\psi_0 - \frac{1}{4\pi r^2}(\Delta_*\delta\psi)\nabla\psi_0, \tag{25}$$

$$\rho_0\partial_t\delta v_\theta = \frac{1}{4\pi r}\mathbf{B}_{\rho_0}\cdot\nabla r\delta B_\theta, \tag{26}$$

where $\delta\psi$, δB_θ, and δv_ρ are perturbations induced by the injection of J_{b_θ}. The $\Delta_*\delta\psi$ terms in the above equations may be omitted for $v_z > v_A$, since the beam current is completely cancelled by the plasma current.[26] With this restriction, the term $\delta v_\theta/r$ may also be neglected in Eq. (24). Combining Eqs. (23) and (25),

$$\partial_t^2\delta\psi = \frac{J_{b_\theta}}{cr\rho_0}|\nabla\psi_0|^2 - \frac{c}{4\pi n_0 e}(\mathbf{B}_{\rho_0}\cdot\nabla)r^2(\mathbf{B}_{\rho_0}\cdot\nabla)\left(\frac{J_{b_\theta}}{n_0 er}\right) + \frac{cr}{\sigma}\partial_t J_{b_\theta}. \tag{27}$$

The second term in this equation is a result of the inclusion of the Hall electric field. The ratio of this to the first term is λ_i^2/a_z^2, where $\lambda_i = c/\omega_i$ is the ion inertial length. This quantity is small for high density plasmas ($n_p \approx 10^{14}$). The ratio of the perturbed toroidal field to the external field strength is approximately $\nu\lambda_i/a_z$. Therefore the neglect of terms to $0(\lambda_i/a_z)$ amounts to the neglect of the perturbed toroidal field. Integrating Eq. (27) with respect to time and substituting the result in Eq. (22), the rate of loss of ring energy is[25]

$$\frac{d}{dt}K = -2\pi\int rdrdz\left(\frac{B_0^2}{c^2\rho_0}J_{b_\theta}\int dtJ_{b_\theta} + J_{b_\theta}^2/\sigma\right). \tag{28}$$

Integrated over time, the loss of energy is[25]

$$\Delta K = K - K_0 = -2\pi\int rdrdz\left(\frac{Q_b^2B_0^2}{2\rho_0c^2} + \frac{1}{\sigma}\int_0^t dt'J_{b_\theta}^2\right), \tag{29}$$

where

$$Q_b(\mathbf{x},t) = \int_0^t dt'J_{b_\theta}(\mathbf{x},t'). \tag{30}$$

Note that the RHS of Eq. (29) is a negative definite. The first term represents the energy expended in displacing the plasma through the $\mathbf{J}_p \times \mathbf{B}$ force. The second term arises from the resistive decay of the plasma return current. The magnitude of the Ohmic loss term relative to wave generation term is

$$\frac{\text{ohmic losses}}{\text{wave generation losses}} = \frac{\tau_A^2}{\tau_\sigma\tau_T} = \frac{c^2v_z}{4\pi\sigma v_A^2a_z}, = R_m^{-1}(v_za_r/v_Aa_z), \tag{31}$$

where $\tau_A = a_r/v_A$, $\tau_\sigma = 4\pi\sigma a_r^2/c^2$, $\tau_T = a_z/v_z$, and $R_m = \tau_\sigma/\tau_A$. To estimate the rate of slowing down, assume a beam current density of the form

$$J_{b\theta}(z,t) = \bar{N}_b(r) e v_\theta a_z^{-1} J\left[(z - Z(t))/a_z\right], \tag{32}$$

where $v_z(t)$ is the mean axial velocity and

$$Z(t) = \int_0^t dt' v_z(t'). \tag{33}$$

Also,

$$\frac{1}{a_z}\int_{-\infty}^{\infty} dz J = 1, \tag{34}$$

and

$$2\pi \int_0^{R_w} r dr \bar{N}_b(r) = N_b. \tag{35}$$

Equation (28) can be employed to obtain

$$\begin{aligned}
\frac{d}{dt}K &= -8\pi^2 \frac{v_A^2}{c^2}\int_0^{R_w} drr \int_{-\infty}^{\infty} \frac{dz}{a_z^2}(\bar{N}_b e v_\theta)^2 J\left(\frac{z-Z}{a_z}\right) \\
&\quad \times \int_0^Z \frac{dZ'}{v_z} J\left(\frac{z-Z'}{a_z}\right) \\
&= -8\pi^2 e^2 \left(\frac{v_A}{c}\right)^2 \frac{1}{v_z} G(Z/a_z) \int_0^{R_w} drr(\bar{N}_b(r) v_\theta)^2,
\end{aligned} \tag{36}$$

where

$$G(Z/a_z) = \frac{1}{a_z^2}\int_{-\infty}^{\infty} dz J\left(\frac{z-Z}{a_z}\right)\int_0^Z dZ' J\left(\frac{z-Z'}{a_z}\right). \tag{37}$$

It has been assumed that $v_z(t)$ changes by a small amount in a time $a_z/v_z(t)$. Also, after the initial transient (i.e. for $Z > a_z$), $G \to 1/2$.

While the ring is axially translating there is no change in the azimuthal energy. This is understood by evaluating the electric field E'_θ in the beam frame using the Lorentz transformation

$$E'_\theta = E_\theta + v_z B_r/c, \tag{38}$$

where E_θ is the electric field in the lab frame. The radial magnetic field is obtained from Maxwell's equation, $\partial_t B_r = c\partial_z E_\theta$. Neglecting transients in the beam frame, the partial time derivative can be replaced by $-v_z\partial_z$. Therefore,

$$B_r = -\frac{c}{v_z}E_\theta, \tag{39}$$

which, when substituted into Eq. (38), gives $E'_\theta = 0$. As long as the ring is moving through the plasma, the energy loss, as calculated from Eq. (36), is subtracted from the translational component of the ring kinetic energy. The ring translational energy is given by

$$K_z = \left(\frac{1}{2}\right) m v_z^2 \int_0^{R_w} 2\pi dr r \bar{N}_b(r). \tag{40}$$

The rate of change of ring energy is

$$\frac{d}{dt}K_z = v_z \frac{d}{dZ}K_z. \tag{41}$$

Substituting Eq. (36) into this, with $G = 1/2$, gives

$$\frac{d}{dZ}v_z^2 = -\frac{1}{v_z^2}\frac{4\pi e^2}{mc^2}v_\theta^2 v_A^2 N, \tag{42}$$

where

$$N = \frac{\int_0^{R_w} dr r \bar{N}_b^2}{\int_0^{R_w} dr r \bar{N}_b}. \tag{43}$$

This has a solution

$$\frac{v_z}{v_{z0}} = (1 - Z/z_A)^{1/4} \tag{44}$$

where the Alfvén slowing down length is given by

$$z_A = \left(\frac{mc^2}{8\pi e^2 N}\right)\frac{v_{z0}^4}{v_\theta^2 v_A^2}. \tag{45}$$

For a 'top hat' shaped radial density distribution of width a_r the following is obtained:

$$z_A = \frac{a_r}{4\nu}\frac{v_{z0}^4}{v_\theta^2 v_A^2}. \tag{46}$$

Hence the scaling of the Alfvén slowing down length with respect to various quantities is $z_A \sim B_0^{-2}$, $v_{\theta 0}^{-2}$, v_{z0}^4, n_p and ν^{-1}. Notice that z_A is independent of a_z; this is because the axial retarding force on the ring particles, $v_\theta \delta B_r/c$, is proportional to Q_b which depends only on the number of particles in the ring. However, since the retarding force on the ring particles is non-uniform along the cross section of the ring, there may be some axial spreading as it slows down.

In order to calculate the ring axial spreading and slowing down, the axial velocity $v_z(z,t)$ is assumed to be a fluid-like quantity. The time dependence of v_z is determined by the Lorentz force arising from the radial magnetic field

$$m\frac{d}{dt}v_z = -\frac{e}{c}v_{b\theta}B_r. \tag{47}$$

The axial electric field $E_z \approx v_{e\theta}B_r/c$ is neglected since it is smaller than the RHS of Eq. (47) by a factor n_b/n_p. The plasma is taken to be infinitely conducting, and there is no initial poloidal ring pressure. The calculation also uses Eqs. (23) and (25) for the perturbed flux and plasma radial velocity. The model is one-dimensional, that is, only axial variations are included, and $v_z > v_A$ so that current neutralization is assumed. As in the above analysis $c^2/\omega_i^2 a_z^2 \ll 1$, therefore the perturbed toroidal magnetic field component is ignored.

Perform a transfer of coordinates to the beam frame

$$z' = z - v_{z0}t \tag{48}$$

$$\tau = t. \tag{49}$$

Then the steady state response ($\partial_\tau \ll v_{z0}\partial_z$) of the perturbed radial magnetic field is

$$B(z) = -\frac{B_0^2}{c\rho_0 v_{z0}^2}\int_\infty^z J_{b\theta}(z'')\,dz''. \tag{50}$$

Equations (47) and (50) along with the continuity equation for ring particles, gives

$$\frac{d}{d\tau}v_z = -\kappa N \tag{51}$$

$$\frac{d}{d\tau}n = -n\partial_z v_z \tag{52}$$

where $\xi = \xi_0 + \int_0^\tau d\tau v_z(\xi_0, \tau)$ is the Lagrangian ring fluid displacement, n is the beam number density so that $J_{b\theta} = nev_\theta$, $\kappa = 4\pi r_{ci}(v_A v_\theta / v_{z0})^2$, and

$$N(\xi_0, \tau) = N(\xi_0, 0) = -\int_\infty^{\xi_0} n(\xi_0', 0)\, d\xi_0'. \tag{53}$$

These equations have solution

$$v_z(\xi_0, \tau) = -\kappa\tau N(\xi_0, 0), \tag{54}$$

$$\xi(\xi_0, \tau) = \xi_0 - (1/2)\kappa\tau N(\xi_0, 0), \tag{55}$$

$$n(\xi_0, \tau) = \frac{n(\xi_0, 0)}{(1 + (1/2)\kappa\tau^2 n(\xi_0, 0))}. \tag{56}$$

From these equations, the following average quantities can be calculated in the beam frame,

$$\bar{v}_z = \frac{\int_{-\infty}^{\infty} d\xi v_z(\xi_0, \tau) n(\xi_0, \tau)}{\int_{-\infty}^{\infty} d\xi n(\xi_0, \tau)} = -2\pi r_{ci} \left(\frac{v_A v_\theta}{v_{z0}}\right)^2 f_r(r)\tau, \tag{57}$$

where $n(\xi_0, 0) = f_r(r) f_z(\xi_0)$, $\int_{-\infty}^{\infty} f_z(z)\, dz = 1$, and $\int_0^{R_w} f_r(r) 2\pi r\, dr = N_b$.

$$\bar{z} = \frac{\int_{-\infty}^{\infty} d\xi\, \xi n(\xi_0 \tau)}{\int_{-\infty}^{\infty} d\xi n(\xi_0, \tau)} = -\pi r_{ci} \left(\frac{v_A v_\theta}{v_{z0}}\right) f_r(r)\tau^2, \tag{58}$$

$$a_{zh} = \left(\frac{\int d\xi (\xi - \bar{\xi})^2 n(\xi_0, \tau)\, d\xi}{\int d\xi n(\xi_0, \tau)}\right)^{1/2} = a_{zho} + \frac{\pi}{\sqrt{3}} r_{ci} \left(\frac{v_A v_\theta}{v_{z0}}\right) f_r(r)\tau^2, \tag{59}$$

where $\bar{v}_z$ and $\bar{z}$ are the respective ring center of mass velocity and position in the frame moving with velocity v_{z0}. Also, a_{zh} is the ring axial half width which is calculated for an initially 'top hat' axial beam shape. The quantity $N(\xi_0, 0)$ is a measure of the number of particles upstream of the fluid element at ξ. Thus Eq. (55) shows that the fluid elements are being slowed self similarly. The axial shape of the ring remains the same but the density is everywhere decreasing in time. Equation (57) shows the dependency of the average velocity

$\bar{v}_z$ on the radial line density. Equation (59) shows that the ring axial half width increases quadratically with time and that the time for this quantity to double is approximately

$$\tau_2 = 2(12)^{1/4}(z_A a_{zho})^{1/2} v_{z0}. \tag{60}$$

In the following, an estimate will be obtained for the effectiveness of an externally imposed toroidal magnetic field on slowing down a translating ion ring. Recall that the radial electric field is responsible for accelerating the plasma ions; this is the mechanism by which energy is imparted to the plasma. This field is given by

$$E_r = \left(v_{ez} B_\theta - v_{e\theta} B_z\right)/c \tag{61}$$

where B_θ is the toroidal field strength at the ring radius. The second term in this expression represents an added contribution above that which occurs when only an axial field is present. The electron velocity in this term arises from the axial beam current neutralization. This will represent a smaller effect, compared with the first since the axial ring velocity is smaller than the toroidal velocity by $\sqrt{f}$. Note that the slowing down now depends on the sign of B_θ.

The expression for the rate of change of ring kinetic energy is

$$\frac{d}{dt} K_b = \int d^3x (E_\theta J_{b\theta} + E_z J_{bz}). \tag{62}$$

From the linearized plasma ion momentum equation, and writing $\mathbf{J}_p = -\mathbf{J}_b$ for $v_z \gg v_A$

$$\rho \partial_t v_{pr} = \frac{1}{c} J_{bz} B_\theta - \frac{1}{c} J_{b\theta} B_z = -\frac{1}{c} J_{b\theta} B_z \left(1 - \frac{v_z B_\theta}{v_\theta B_z}\right). \tag{63}$$

Therefore, the first term on the RHS of Eq. (62) becomes

$$\int d^3x E_{b\theta} J_{b\theta} = -\int r\, dr\, dz 4\pi^2 \left(\frac{v_A}{c}\right)^2 \left(1 - \frac{v_z B_\theta}{v_\theta B_z}\right) J_{b\theta} \int dt J_{b\theta} \tag{64}$$

where $v_A = B_z/\sqrt{(4\pi\rho)}$. For the second term, the axial electric field is

$$E_z = \left(v_{e\theta} B_r - v_{er} B_\theta\right)/c. \tag{65}$$

The ratio of the first to the second of these terms is approximately $(n_p/n_b)(B_\theta/B_z)\sqrt{f}$. Thus, the first term dominates for the case of a low density beam. With the assumption $c/\omega_i a_r \ll 1$, the perturbed toroidal magnetic field can be neglected. Therefore, from Ampere's law the radial electron and plasma ion velocities are approximately equal, so that

$$E_z \approx -v_{pr} B_\theta / c. \tag{66}$$

The second term on the RHS of Eq. (62) becomes

$$\int d^3x E_z J_{bz} = -\int r\, dr\, dz 4\pi^2 \left(\frac{v_A}{c}\right)^2 \left(\left(\frac{v_z B_\theta}{v_\theta B_z}\right)^2 - \frac{v_z B_\theta}{v_\theta B_z}\right) J_{b\theta} \int dt J_{b\theta} \tag{67}$$

Putting the two equations (64) and (67) together and integrating to get the total change in ring energy, gives

$$\Delta K_b = -\int r\, dr\, dz 4\pi^2 Q^2 \left(\frac{v_A^2}{c}\right) \left(1 - \frac{v_z B_\theta}{v_\theta B_z}\right)^2. \tag{68}$$

The condition for the enhancement of slowing down in the presence of a toroidal magnetic field is $v_z B_\theta / v_\theta B_z < 0$.

Performing a similar calculation as before, an expression for the axial position of the ring as a function of v_z obtained:

$$\begin{aligned} Z(v_z) &= \frac{a_r}{\nu}\frac{v_{z0}^2}{v_A^2}\frac{B_z^2}{B_\theta^2}\left(\frac{1}{2} + \frac{2}{\Delta} + \frac{1}{\Delta^2}\left(\frac{1}{1-\Delta} + 3\ln(1-\Delta)\right)\right) \\ &\quad - \frac{1}{2}\left(\frac{v_z}{v_{z0}}\right)^2 - \frac{2}{\Delta}\frac{v_z}{v_{z0}} \\ &\quad - \frac{1}{\Delta^2}\left(\frac{1}{1-\Delta\frac{v_z}{v_{z0}}} + 3\ln\left(1 - \frac{v_z}{v_{z0}}\Delta\right)\right) \end{aligned} \tag{69}$$

where $\Delta = (B_\theta v_{z0}/B_z v_\theta)$. The slowing down length is

$$\begin{aligned} Z(v_z = 0) &= \frac{a_r}{\nu}\frac{v_{z0}}{v_A^2}\frac{B_z^2}{B_\theta^2}\left(\frac{1}{2} + \frac{2}{\Delta} + \frac{1}{\Delta^2(1-\Delta)} + \frac{3}{\Delta^2}\ln(1-\Delta)\right) \\ &= \frac{a_r}{4\nu}\frac{v_{z0}^4}{v_\theta^2 v_{Az}^2} \qquad \text{when } \Delta \ll 1, \\ &= \frac{a_r}{4\nu}\frac{v_{z0}^2}{v_A^2}\frac{B_z^2}{B_\theta^2} \qquad \text{when } \Delta \gg 1. \end{aligned} \tag{70}$$

This analysis assumes that all of the energy going into the plasma comes from the axial translational ring energy. Since the toroidal field perturbs the single particle orbits in the poloidal plane, this assumption is valid only in the limit $\Delta \ll 1$.

C. General Discussion on Slowing Down Lengths

In an earlier work by the present authors, typical slowing down lengths in a resistive plasma ($R_m \lesssim 1$) were calculated[7]. Two regimes are appropriate for the velocities where $v_z \gtrless v_c$, where $v_c = v_A R_m^{-1}(a_r/a_z)$,

$$z_a = v_{z0}\tau_a \qquad v_z < v_c \tag{71a}$$

$$z_b = \frac{2}{3} v_{z0}\tau_b[1-(v_c/v_0)^2] \qquad v_z > v_c, \tag{71b}$$

where $\tau_a = 2c^2 a_z/(a_r^3 \sigma \nu \Omega^2)$, $\tau_b = (\pi^2/4)(a_r a_z/R_b^2)(v_0/c)^2\sigma/(\nu\Omega^2)$, $\Omega = eB_z/m_p c$. From the discussion in section B, we know that in a conductive plasma the scale lengths that are relevant are z_A, Eq. (46) and z_b, and that the former is applicable when $z_b/z_A = R_m v_A a_z/(v_z a_r) \gg 1$.

Another important regime corresponds to the removal of axial translational energy in a conductive plasma when $v_z < v_A$. A crude estimate for the slowing down length in this regime can be obtained as follows. As the ring translates through the plasma, the self fields perturb the uniform external field. In a conductive plasma, the plasma ions move radially with the field lines through a distance

$$\delta r = \zeta R_b. \tag{72}$$

The time for this displacement to occur is approximately the ring transit time, a_z/v_z. Assuming that the energy imparted to the plasma motion is not fed back to the ring, the rate of change of ring energy can be estimated from conservation of energy. The result is

$$\frac{d}{dt}K_b = -\frac{\pi}{4}\frac{R_b^3 a_r}{a_z^2}\zeta^2 B_0^2 \frac{v_z^3}{v_A^2}. \tag{73}$$

Following the discussion of section B, the energy is assumed to be removed from the ring translational kinetic energy. The axial velocity as a function of time is easily solved for:

$$v_z = v_{z0}/(1 + t/\tau), \tag{74}$$

where $\tau = 4a_z^2 v_A^2/v_{z0}\pi\zeta a_r v_\theta^2$. The Alfvén slowing down length $z_A^{(1)}$, for $v_z < v_A$, can be obtained by integration; $\int^\tau v_z\, dt$:

$$z_A^{(1)} = \frac{4}{\zeta\pi}\frac{a_z^2}{a_r}\frac{v_A^2}{v_\theta^2}. \tag{75}$$

It should be noted that when $v_z < v_A$, steady state Alfvén wave generation does not occur. This weakens the assumption that energy is removed from the translational component of the ring kinetic energy. Indeed, in regime $v_z < v_A$, the theta kinetic energy is being transferred to the energy in the ring self fields. Therefore, the application of Eq. (74) to experimental situations should be guarded.

III. Particle Code Simulations

A. Ring Translation in an Axial Magnetic Field

The simulations were performed using the hybrid code CIDER.[27] Ions that make up both the energetic rings and the background plasma are modeled as particle in cell (PIC), and the electrons are treated as a fluid. The transverse displacement current in Maxwell's equations is neglected, thus eliminating the speed of light as a determinant of the code timestep. Also, the electron mass in the momentum equation is neglected and quasineutrality is assumed. With these conditions, the two strongest limitations on the timestep comes from the Courant condition $k_{\max} v_A \Delta t < 1$, where $k_{\max}$ is the maximum wave number represented and the particle integrator accuracy condition $\Omega_i \Delta t < 1$. Note that the Courant condition is appropriate since it is Alfvén wave activity that we want to model. Since CIDER uses an explicit algorithm to advance the physical quantities in time, the Courant condition determines not only accuracy but also a numerical stability limit.

A typical ring is shown schematically in Fig. 1. The parameter of a base run are: wall radius $R_w = 150$ cm, total axial length $z_w = 900$ cm, $R_b = 75$ cm, $N_b = 2.0 \times 10^{17} (\nu = 0.41)$, $B_{z0} = 1.7$ kg, $n_p = 5.0 \times 10^{13}$ cm^{-3}, and $v_{z0} = 4.2 \times 10^8$ cm s$^{-1} (v_{z0}/v_A = 8)$. For the moment we are considering only slowing down in a uniformal axial magnetic field. The numerical grid is $30(R) \times 40(z)$. With these parameters, the upper limit on the timestep is $\Delta t = 5ns$ which gives $k_{\max} v_A \Delta t = 0.33$ and $\Omega_i \Delta t = 0.08$. If a timestep much larger than this is used the code fails to conserve energy and ultimately becomes unstable. The ring is initialized with no poloidal temperature. Figure 2 shows, for the base run, selected particle positions in the poloidal plane at various times. Notice that the axial width of the ring increases throughout the run, this is caused by the nonuniform axial stopping force $F_z \sim J_b \delta B_r$ across the ring; varying from zero for particles at the head of the ring up to a maximum for particles at the rear. Careful observation shows that the particles in the front of the ring are not slowed whereas those behind are slowed successively more and more. This process takes place until $v_z \leq v_A$, when self fields envelop the whole ring. Fig. 2(g) shows the poloidal field lines, including the self field perturbation, at time $t = 2.5\mu$s. Note that there is some radial dependency of the slowing down rate; those particles in the center of the ring, where the density is highest, are slowed to a greater extent than those at the inner and outer radii. For the run shown in Fig. 2, approximately one half of the particles were fully stopped and the remaining escape.

Figure 3(a) shows, for the base run, a plot of the ring axial translational energy against time. The slowing down occurs during the first microsecond, after which the particles at the front of the ring start to pass out of the system. Fig. 3(b) shows the total toroidal energy of the ring particles. During the period of slowing down there is very little change in this energy. This verifies the assumption made in the above analysis that the energy is removed only from the axial component of the translating ring. The sudden drop in energy at the end of the run is due to the loss of particles at the right hand wall.

A number of runs were performed with varying v_{z0}/v_a. In accordance with Eq. (44), the slowing down length z_s is measured by taking the length scale from a plot of v_z^4 against z. Figure 3(c) shows such a plot for the base run. Note that the radial magnetic field, which acts to slow down the beam ions, is only generated after the beam transits across itself. Thus the slowing down does not begin until the ring has traveled a distance a_z. The slowing down length for this run is 257 cm compared with the theoretical estimate z_a=237 cm. Table 1 shows the measured slowing down lengths compared with the theoretical estimate z_A for the range of initial axial ring translational velocity $v_{z0}/v_A = 1.0$ up to 14.1. The assumptions that went into the theory breakdown for $v_z \sim v_A$, and this is clearly borne out here.

According to Eq. (46), the slowing down length scales as v_z^4. This scaling is checked using Fig. 4(a), which is a plot of log (z_s) against $\log v_{z0}/v_A$. The gradient of the curve, for $v_{z0}/v_A \gg 1$, is 3.41 compared with the theoretical result of 4. When $v_{z0}/v_A \sim 1$, the measured slowing down length is considerably in excess of z_A. This is clearly demonstrated in Fig. 4(b), which is a plot of $\log(z_s/z_A)$ against v_{z0}/v_A. Note that the axial grid spacing for that run is 5 cm so that the first point on the curve in Fig. 4(b) is close to the limit of numerical resolution.

A series of runs was performed using the code CIDER to test the theoretical results of the one-dimensional ring fluid model. This model includes both the axial slowing down and the axial spreading of the ring. The same general physical parameters are used as for the runs which are described earlier in this section. These runs were intended specifically to test the power law dependency in the expression

$$\frac{d}{d\tau}\bar{v}_z \sim \frac{N_b}{a_r}\frac{B_0^4}{v_{z0}^2}\frac{1}{n_p} \tag{76}$$

Figure 5(a)-(f) shows plots of $\log d\bar{v}_z/d\tau$ against the logarithms of ν, B_0, a_r, a_z, v_{z0}/v_A, and n_p, respectively. The theoretical exponents are checked against the gradients of straight line fits to the curves. The results are summarized in Table 2. The points which do not

fall on the straight lines correspond to some limit in which the above analysis is not correct. Therefore, in Fig. 5(a) the deviation corresponds to the large number of particles ($\nu > 1$), so that the self fields are of the order of the external fields. This breaks the linearity approximation used in the theory. In Fig. 5(e) the deceleration is diminished for $v_{z0}/v_A \sim 1$ as discussed earlier in this section. Finally, at low density in Fig. 5(f), the same situation pertains as when $v_{z0}/v_A \approx 1$.

For the run shown in Fig. 3, a number of quantities can be checked. Firstly, as mentioned earlier, the slowing down length is measured to be 257 cm compared with $z_A = 234$ cm. The initial deceleration of the ring as calculated from Eq. (57) is -1.83×10^{14} cm s^{-2}, while the measured value is -2.37×10^{14} cm s^{-2}. Finally, the time taken for the ring axial half width to double is calculated from Eq. (60) to be 0.76μ s, while the measured time is 0.98μ s.

B. Ion Ring Translation in an Axial and Toroidal Magnetic Field

For the case where a toroidal magnetic field is present, a number of simulations were performed using a single particle version of CIDER. A uniform axial field was imposed, as well as a toroidal field with $1/r$ radial dependence. The results are summarized in Fig. 6(a) and (b) which show the average axial velocity $\langle v_z \rangle$, as taken from the simulation, (solid curve) as well as the theoretical drift velocity v_D (dashed curve). The plot shown in Fig. 6(b) is an enlargement of the region $B_{\theta b}/B_z < 0$. This clearly shows the opposing drifts as expressed in Eq. (11). The theoretical drift velocity is shown to be approximately correct outside of the limits set by $B_{\theta 3}$ and $B_{\theta 4}$. In the regime where $|B_{\theta b}/B_z| > 1$, the guiding center theory is clearly inapplicable, and the ratio $\langle v_z \rangle / v_{z0}$ tends to unity as the toroidal field vanishes.

A set of runs was also performed to assess the role played by the toroidal magnetic field on the removal of ring translational energy. For this, the fully self-consistent version of CIDER was employed, and the same parameters were used as for the slowing down runs in Section A. An external $B_\theta \sim 1/r$ was imposed by passing a current along an axial conductor.

The ratio of the initial parallel ring velocity to the Alfvén speed was $v_{z0}/v_A = 10.2$; therefore $f = 0.18$. This makes the run very similar to RUN#5 in Table 1. The values of $|B_\theta/B_z|$ were 0.0, 0.25, 0.5, and 1.0. For $v_{z0} > 0$ and $B_z > 0$, a positive toroidal field corresponds to an enhancement in the ring translational energy loss.

Table 3 summarizes the results of the present series of runs. The quantity

$$\xi = \left(1 - \frac{v_z B_\theta}{v_\theta B_z}\right)^2 \tag{77}$$

appears inside the integrand in Eq. (67); it is a measure of the contribution of the toroidal field to the removal of ring kinetic energy. The quantity δE_b is the rate of change of ring energy measured just after it has traveled an axial distance a_z; the results are normalized to the rate for RUN#1. This quantity should be equal to ζ. It can be seen that the comparison is good, especially where $|B_\theta/B_z|$ is small. For these runs where the fast ions are collisionless and the plasma resistivity is zero, the total field and particle energy should be conserved. Figure 7(a), (b) and (c) show plots of the total energy (less the energy of the externally imposed magnetic fields) against time for RUNS#1, 3 and 6, respectively. In RUN#1 the energy is constant up to a few percent until $t = 1.5\mu$s, when the ring particles start to be absorbed at the right hand wall. However, in the remaining two plots the energy steadily increases before particle absorbtion occurs. The quantity ϵ, which is shown in Table 3, is the amount of excess energy divided by the energy exchanged between the ring and the plasma waves. It is measured during the same time period that the quantity δE_b is evaluated. This shows that RUN'S# 1, 2, 5 and 6 are reliable, however the others are in doubt due to energy non-conservation. This occurs when the code becomes numerically unstable or inaccurate. The quantities $k_m v_A \Delta t$ and $k_m^2 v_A^2 \Delta t/\Omega_i$ must be less than unity to ensure numerical accuracy and stability. As the toroidal field is increased these factors also increase, and in some cases they exceed unity. The RUN#7 was repeated with a reduced timestep such that $k v_A \Delta t = 0.08$ and $k^2 v_A^2 \Delta t/\Omega_i = 0.33$. However, the quantity $\epsilon = 43\%$ represented only a slight improvement.

The lack of energy conservation is probably a combination of the timestep constraint and the tendency for numerical noise to develop due to the sharp B_θ contour close to the current carrying conductor on axis.

Figure 8(a), (b) and (c) shows the plots of the tracer particle orbits in the poloidal plane for RUNS#1, 3 and 6, respectively. In the first plot, where there is no external toroidal magnetic field, there is no radial motion of the ring prior to its slowing down. The second plot, where $B_\theta/B_z = 0.5$, corresponds to a reduction in the slowing down length compared with RUN#1. The orbit is initially axial; however the toroidal magnetic field soon deflects the particle toward the axis. Thereafter, it travels with a cusp-like trajectory. From the theory presented in Section II, the cusped motion occurs when $B_\theta/B_z = \sqrt{f}/(1-\sqrt{(f+1)}+\sqrt{f} = -0.831$.

In deriving Eq. (68), the radial and toroidal components of the ring energy were taken to be constant. Thus, the energy that is transferred to the plasma waves was assumed to be removed only from the axial translational energy $N_b(1/2)mv_z^2$. Therefore, the result is correct when $\Delta \ll 1$. In this limit the expression for the slowing down length [Eq. (69)] is

$$z_A = \frac{a_r}{4\nu}\frac{v_{z0}^4}{v_A^2 v_\theta^2}\left(1+\frac{8}{5}\Delta+\cdots\right). \tag{78}$$

The slowing down lengths were measured for RUNS#1, 2 and 5; where $\Delta = 0, -0.11$ and 0.11, respectively. Figure 9(a), (b), and (c) shows the respective plots of $(v_z/v_{z0})^4$ against Z. Note that the plots (b) and (c) show oscillations due to the cusp-like ring trajectory in the poloidal plane. For these cases, the slowing down length z_s can be calculated by taking the scale length from a line which connects the peaks of the oscillations. Table 4 summarizes the results. The quantity α is the slowing down length z_s normalized to the length for RUN#1. The sign of the toroidal field is found to have the predicted effect on reducing or increasing z_s.

The situation where $k_z c/\omega_i > 1$ ($k_z = 2\pi/a_{zh}$) is relevant when there is a low plasma

density or the axial length of the ring is small. This is the regime where the Hall electric field ($\mathbf{J}_p \times \mathbf{B}/n_p ec$) in Ohm's law becomes important; the toroidal magnetic field which is generated by the motion of the ring can no longer be neglected, and the above analysis for slowing down is not strictly correct. Computationally, this is a difficult problem because the usual Courant condition becomes modified by a factor $k_{\max} c/\Omega_i \gg 1$. This puts a much greater restriction on the timestep, thus increasing the CPU time requirement.

A number of simulations were performed to assess the effect of the Hall field on the slowing down lengths. The initial axial translational velocity of the ring was $v_{z0} = 2.5 v_A$. The results are summarized in Table 5 which shows the measured slowing down length z_s divided by the calculated length z_A. The factor $k_z c/\omega_i$ is adjusted by changing either the ring axial half width a_{zh}, or the ion plasma frequency ω_i. In order to keep z_A invariant for these runs, the Alfvén speed was not altered. Thus, for the purpose of varying ω_i, the ratio n_p/m_i was changed while $n_p m_i$ was held fixed (m_i is the plasma ion mass). The last column in the table shows the ratio of the toroidal magnetic field energy to the poloidal field energy generated during the run. This gives a measure of how much the increase in the quantity $k_z c/\omega_i$ generates greater toroidal field perturbations. For the last run, the magnetic field energy is almost equally distributed between the three components. For the parameters indicated, the results show that the increase in $k_z c/\omega_i$ to a value greater than unity does not substantially alter the slowing down length.

IV. Coalescence of a Weak Ring with a Field Reversed Configuration

In this section we consider the dynamics of a weak ion ring, $\zeta < 1$, in the vicinity of a field reversed configuration. Because the background plasma is taken to be highly conductive, the code CIDER was employed. However, this code can only be used to simulate processes which take a small number of Alfvén transit times R_w/v_A of the system, where R_w is the

wall radius of the confining cylinder. Because of restrictions on computer time, and because the code is inherently noisy, it would be impossible to simulate the whole process of ring formation, translation, and merging. Hence the initial ring particle-field configuration was established using the RINGA[28] code. This code may be employed where the plasma is highly collisional. RINGA uses about one third as much computer time as CIDER for an equivalent run, and since it is an implicit code it provides a more noise free simulation. The FRC was established using an axisymmetric force-free spheromak equilibrium.[29] This is suitable for use in CIDER because the force-free current is carried by the fluid electrons. Therefore, the electric field, which can generate noise by perturbing the plasma ions, is identically zero.

The expression for a force free magnetic field is

$$\nabla \times \mathbf{B} = \kappa \mathbf{B}. \tag{79}$$

The quantity κ is nonzero inside of a sphere of radius r_0, corresponding to the location of the spheromak. Elsewhere κ is zero, corresponding to vacuum magnetic fields. In spherical coordinates (ρ, θ, φ) the fields inside of the sphere are given by

$$\begin{aligned} B_\rho &= 2b_1 P_1^0 j_1(k\rho)/k\rho, \\ B_\theta &= -b_1 \sin\theta P_1^{0\prime}(r j_1(k\rho))'/kp, \\ B_\varphi &= b_1 \sin\theta P_1^{0\prime} j_1(k\rho), \end{aligned} \tag{80}$$

where $P_1^0(z) = z$, $j_1(z) = \sin(z)/z^2 - \cos(z)/z$ and $kr_0 = 4.493$. Outside of the sphere the vacuum field is given by

$$\mathbf{B} = B_0 \nabla \left\{ (\rho + r_0^3/2\rho^2) P_1^0(\cos\theta) \right\}, \tag{81}$$

which tends to a solenoidal field B_0 at large ρ. The matching condition at the boundary gives $b_1 = 3kr_0 B_0/2\sin(kr_0)$. These fields were initialized in the cylindrical (r, θ, z) code CIDER.

As noted by Rosenbluth and Bussac,[30] there are no unstable surface modes at r_0 for the above axisymmetric field solution. This is important because it is necessary to avoid instabilities which would cloud the interpretation of the coalescence runs.

For the simulations which are presented in this work, the wall radius was chosen to be 150 cm, the separatrix was $r_0 = 100$ cm, the axial length of the system was 450 cm, and the spheromak was located at $Z_s = 300$ cm. The external magnetic field B_0 was set ot 1.7 kG; this determines that the peak magnitude of the toroidal magnetic field is 5.0 kG, and the magnitude of the axial magnetic field on axis, at the position of the spheromak, is 7.83 kg. Figure 10(a) show the resulting poloidal field line configuration, while (b) shows a Contour plot of the toroidal magnetic field. Once again, the numerical grid the used for the $30(r) \times 40(z)$. The density in the vacuum region was 4.5×10^{13} cm^{-3}, and the timestep of the runs was $\Delta t = 5$ ns; this gives the accuracy-stability conditions $k_{\max} v_A \Delta t = 0.35$, $k_{\max}^2 v_A^2 \Delta t / \Omega_i = 1.5$ and $\Omega_i \Delta t = 0.081$ to 0.37. The density is artificially increased in the vicinity of the spheromak so as to keep $k_{\max} v_A \Delta t$ from increasing, and approaching the Courant stability limit of unity. It was found that the code failed to conserve energy when the ring entered the spheromak. This was traced to the increase in $\Omega_i \Delta t$ due to the large toroidal magnetic fields there. The particle integrator became inaccurate since there were not enough timesteps to resolve their strongly curved ion trajectories. This problem was eliminated by reducing the timestep to $1\,ns$ as the ring entered the spheromak.

A very weak ring ($\zeta \ll 1$) can be considered as being a collection of single particles in the sense that the self fields of the ring, being very weak, do not affect the particle dynamics. In Section II it was shown that the potential H^* determines the accessible area for the motion of an ion in the r, z plane, as expressed in the following

$$(1/2)mv_\rho^2 + H^* = \text{const.} \tag{82}$$

where $\mathbf{v}_\rho$ is the velocity of the ion in the r, z plane. Furthermore, this result holds true even

in the presence of a theta magnetic field. Also, when there are a finite number of particles, the self field perturbation must be weak enough so that $\partial_t H^* \ll \mathrm{v}_\rho \cdot \nabla H^*$. An extensive discussion of charged particle motion in field reversed configurations is given by Lovelace.[22] For the fields which are used in the present work, as specified by Eqs. (80) and (81) and for a particle that is injected at $r = 75$ cm. a large distance away from the spheromak, the contours of H^* are plotted in Figure 11. It can be seen that the contours are mirror symmetric about the axial position of the spheromak at $Z_s = 300$ cm.

By way of instruction, a number of single particle orbits were calculated. A single particle version of the code CIDER was used for this purpose. The loci of these orbits in the r, z plane are shown in Figure 12. The particles were injected with velocity $v_z = 0$, $v_r = 0$, and $v_\theta = r\Omega_0$, with initial positions $z_i = 70$ cm, and $r_i = 35,\ 45,\ 55,\ 65,\ 75,\ 85,\ 95,\ 105$ cm. Clearly, the accessible area includes the initial point and the mirror image of the injection point on the other side of the spheromak. For particles injected near the midplane, $r = 75$, the accessible area does not intersect with the outer wall. The toroidal field does not alter the accessible area, however it does alter the trajectory of the particles in that area. The particle which is injected at $r_i = 55$ shows a significant radial jump, due to the $\mathrm{v}_\rho \times \mathbf{B}_\theta$ force, as it passes through the spheromak. The accessible area of particles which are injected at larger radii includes the radial wall. It can be seen in Fig. 12 that some of these particles do pass very close to the wall.

A ring with finite self fields is expected to show some deviation from single particle behavior. In another paper by the present authors[7], in relation to the merging of ion rings in a resistive plasma, it was shown how the self flux of a weak ion ring creates a shallow well in the local potential H^*. The depth of the well is approximately ζK_0, where $K_0 = (1/2)m(R_b\Omega)^2$, where R_b is the ring radius, and $\Omega = eB_0/mc$. Also this quantity, ζK_0, is approximately the amount of kinetic energy which is transferred between the particles and the self fields during injection. Using the RINGA-CIDER interface, a ring with field reversal factor $\zeta = 0.25$

was initialized at $Z_b = 120$ cm. and $R_b = 75$ cm., in the spheromak fields which were specified above. Figure 13 shows the resulting contour plot of H^*. Note that the canonical angular momentum $\langle P_\theta \rangle$, which is used in the expression for the potential, is taken to be the algebraic mean over the set of simulation particles. The manner in which the average is taken is not important because the ring is injected with a large aspect ratio, and the particles have a small spread in initial velocity, so that the spread in canonical angular momentum is minimized. Figure 13 clearly shows the shallow well of the incoming ring to the left of the potential well of the spheromak. This shallow well corresponds to the self fields of the ring which prevent it from spreading axially. The weak ring is attracted toward the spheromak, and it moves axially along with its self fields. As it approaches the spheromak, the strong magnetic fields of the latter will cancel the self field of the ring in the region between them. This corresponds to a diminishment of the potential H^* in that region. A point will be reached in the motion of the ring where its particles will become deconfined from the self fields, and they will "spill out" into the spheromak. From the point where they spill out, until they coalesce with the spheromak, the ions perform single particle motion, since the magnetic fields are static during that time.

The spill-out position can be estimated by finding the axial position where the radial self field at the leading edge of the ring is equal to the radial field of the spheromak. At that point the net radial magnetic field, which is responsible for the axial confinement of the particles, is zero. The self flux threading the ring is approximately

$$\delta\psi_s = \pi R_b^2 \zeta B_0. \tag{83}$$

Next, assume that this flux passes through half of the ring axial cross section at the ring radius; so that

$$\delta\psi_s = 2\pi R_b \left(\frac{a_z}{2}\right) B_r, \tag{84}$$

where a_z is the axial cross-sectional width of the ring. Finally, use the divergence free nature

of the magnetic field to estimate the radial field of the spheromak in terms of the axial derivative of the axial magnetic field

$$B_r^{ex} \approx -R_b \partial_z B_z^{ex}. \tag{85}$$

Using the above three expressions, the spill-out condition can be given in terms of the strength of an incoming weak ring below which the particles will spill out of their self fields

$$\zeta_c = \frac{a_z}{B_0} \partial_z B_z^{ex}. \tag{86}$$

Four runs illustrate the above behavior. The basic configuration of the runs has been described above, while the specific characteristics of each run are given in Table 6. The initial field reversal factor of the run is ζ; the axial position of the ring at injection is Z_0; the initial value of translational velocity is v_{z0}; the initial value of the critical field reversal factor is ζ_c; NABS is the percentage of particles which are absorbed at the right hand wall after the ring coalesces with the CT.

For RUN#1, the ring was initialized with a translational velocity so that the particles immediately separated from the self fields, and coalesced with the spheromak. For RUN#2, the ring was initialized with no translational velocity, but its self fields were sufficiently weak, and it was close enough to the spheromak so that spill out occurred immediately. In contrast with this, the ring self fields for RUN#3 were stronger so that $\zeta_c/\zeta \ll 1$, and the point of injection was further from the spheromak so that the ring had to move some distance before spill out occurred. RUN#4 was similar to RUN#3, except that there were fewer particles in the ring ($\zeta_c/\zeta \gg 1$), so that spill out occurred immediately. The time development of RUN#3 is illustrated in Figure 14(a) and (b). Plot (a)shows the poloidal magnetic field lines. The self field perturbation can be seen to travel with the ring, and is then left behind after spill out occurs. Plot (b) shows selected ring particle positions in the (r, z) plane as the ring moves closer to, and is then trapped inside the spheromak. Figure 15

shows an axial cross-section of the potential H^* at the ring radius before (solid line), and after (dashed line) coalescence. After spill out, the magnetic field perturbation convects away, and the potential restores almost to its initial state. This represents a barrier to the return of individual particles to their initial positions.

Figure 16(a) and (b) shows plots of the average ring translational speed, normalized to the Alfvén speed, against time. Plot (a) shows the velocities for RUN#1 and 2, while (b) shows the plots for RUN#3 and 4; the plots (a) and (b) are separated for clarity only. The plots for RUN#1, 2, and 4 show that the rings are never confined by their self fields. For RUN#1, the ring was injected with a large translational velocity, while RUN#2 and 4 and $\zeta < \zeta_c$. For RUN#3, the ring builds up axial speed steadily, and only exceeds the Alfvén speed late in the run when it enters the spheromak.

The number of particles absorbed at the right hand wall is a measure of how well the ring coalesces with the spheromak. The RUN#3 can be directly compared with RUN#4. Figure 17(a) and (b) shows the initial accessible area in the poloidal plane for these two runs. The ring in RUN#3 is stronger and therefore the particles lose more energy due to the creation of the field energy. This leads to a reduction in the poloidally accessible area compared with RUN#4. Comparing the kinetic energy of the two rings on initialization (after their self fields have formed), the particles in RUN#3 have 10% less energy than RUN#4. In RUN#4 the ring was weak enough so that spill out occurred immediately; the particles performed essentially single particle orbits, and the accessible area of these, by reason of their higher initial energy, includes the right hand wall.

The improved confinement of ring particles in RUN#3 seems to arise from their sitting at a lower H^* contour due to the creation of self fields. A second phenomenon might be operating. The increasing axial width of the ring as it enters the spheromak means that it is unlikely to tunnel, with its self fields, through the potential barrier to the wall. Note that while spill out occurred early in RUN#2, the small number of particles absorbed at the wall

is due to the initialization of the ring close to the spheromak with no axial velocity, so that the accessible area was smaller.

V. Conclusion

We have completed a numerical study of ion ring dynamics in highly conductive plasmas. For the translation of a ring in a uniform axial magnetic field faster than the Alfvén speed, a slowing down length $z_A = (a_r/4\zeta)v_{z0}^4/(v_\theta^2 v_A^2)$ has been derived analytically, and verified using the hybrid particle code CIDER. We have also considered the dynamics of weak ($\zeta < 1$) rings in the vicinity of a field reversed configuration. The results agree with the conclusion of a previous paper by the present authors[7] that a stronger incoming ring in more effective in terms of the number of particles that are ultimately confined. In particular, if the translational energy of that ring is greater than ζk_0 (where k_0 is the theta kinetic energy) then the ring will be unconfined. In that case, one way to improve the situation would be to translate the ring over one of the relevant collisional or collisionless slowing down lengths, as discussed in Sec. IIC, before attempting coalescence. In a highly conductive plasma, an added aspect is that a ring that translates with its self fields will travel not faster than the local Alfvén speed. This is true up to the spill out position where the field reversed factor equals a critical value, $\zeta_c = (a_z/B_0)\partial_z B_z$. Beyond that point the dynamics are described by single particle orbits in a static magnetic field.

Recently an experiment on translating ion rings in conductive plasmas has been completed at Cornell University.[13] Magnetic oscillations that are characteristic of magnetosonic (Alfvén) waves were observed. The energy that was transferred between the beam and plasma was consistent with the expression derived by Peter and Rostoker,[11] however the field reversal factor was sufficiently small ($\zeta \approx 0.01$) so that no unequivocal statement could be made as to which of the resistive or Alfvénic slowing down lengths was operable.

Finally, we note a difference between the above slowing down mechanisms and the process

by which a ring is reflected from a magnetic mirror. In the latter, the particles at the front of the ring may be reflected, but the field perturbation that they generate may allow subsequent particles to pass through. In the case of the Alfvénic or resistive slowing down mechanism, the particles in the front of the ring may pass out of the system while succeeding particles are slowed down. The apparent paradox is resolved by recognizing that in both cases the first particles perform single particle orbits; the latter particles have orbits that are determined by both the external and the self consistent magnetic fields.

Acknowledgements

The authors would like to acknowledge our discussions with Dr. E. Schamiloglu, Dr. A. Mankofsky and Dr. D.A. Hommer. The computing was performed on the NMFECC computers in Livermore, California. This work was funded by the U.S. Department of Energy Contract No. DE-FG05-80ET-53088.

References

(1) R.N. Sudan and E. Ott, Phys. Rev. Lett. **33**, 355 (1974).

(2) H.H. Fleischmann, Ann. N.Y. Acad. Sci. **251**, 472 (1975).

(3) R.N. Sudan and P.K. Kaw, Phys. Rev. Lett. **47**, 575 (1981).

(4) P.L. Dreike, J.B. Greenly, D.A. Hammer, and R.N. Sudan, Phys. Fluids **25**, 59 (1982).

(5) E. Schamiloglu (submitted to Phys. Fluids).

(6) R.E. Hester, G.D. Porter, B.W. Stallard, J. Taska, C.W. Walker, and P.B. Weiss, Phys. Fluids **18**, 96 (1975).

(7) P.M. Lyster and R.N. Sudan, Phys. Fluids **31**, 3760 (1988).

(8) K. Molvig, and N. Rostoker, Phys. Fluids **20**, 444 (1979).

(9) K.R. Chu and N. Rostoker, Phys. Fluids **17**, 813 (1974).

(10) K. Molvig and N. Rostoker, Phys. Fluids **20**, 504 (1977).

(11) W. Peter and N. Rostoker, Phys. Fluids **28**, 1532 (1985).

(12) C.W. Roberson, Nucl. Fusion **18**, 1693 (1978).

(13) E. Schamiloglu, PhD Thesis "Proton ring translation in a Magnetized Plasma," Cornell University, May, 1988.

(14) C.A. Kapetanakos, W.M. Black, and C.D. Striffler, Appl. Phys. Lett. **26**, 368 (1975).

(15) W.C. Condit and R.V. Lovelace, Phys. Fluids **17**, 1719 (1974).

(16) G.D. Porter and B.W. Stallard, Phys. Fluids **17**, 1722 (1974).

(17) R.J. Briggs, R.E. Hester, G.D. Porter, W.A. Sherwood, R. Sporlein, B.W. Stallard, J. Tasaka, and P.B. Weiss, *Astron. Program Final Report*, Lawrence Livermore National Laboratory Report UCRL-51874 (1975).

(18) H.A. Davis, D.J. Rey, and H.H. Fleischmann, Phys. Rev. Lett. **39**, 744 (1977).

(19) H.H. Fleishmann, (Private Comm 1986).

(20) R.V. Lovelace, Phys. Fluids **22**, 542 (1979).

(21) N.A. Krall and A.W. Trivelpiece, *Principles of Plasma Physics*, (McGraw-Hill, 1973).

(22) S.I. Braginskii, *Reviews of Plasma Physics*, **1**, 205 (1965) (Consultants Bueau, N.Y.).

(23) R.N. Sudan and P.M. Lyster, Comments Plasma Phys. Controlled Fusion **9**, 23 (1984).

(24) H.L. Berk and L.D. Pearlstein, Phys. Fluids , **11**, 1831 (1976).

(25) A. Mankofsky, J. Denavit, and R.N. Sudan, J. Comp. Phys.

(26) A Masnkofsky, A. Friedman, and R.N. Sudan, Plasma Phys. **23**, 521 (1981).

(27) G.K. Morikawa, Phys. Fluids **12**, 1648 (1969).

(28) M.N. Rosenbluth and M.N. Bussac, Nucl. Fusion **19**, 489 (1979).

Figures

(1) Physical setup of a translating ion ring in an external magnetic field B_0.

(2) Particle positions for the base slowing down run (a) $t = 0$ (b) 0.5, (c) 1.0, (d) 1.5 (e) 2.0 (f) 2.5μs. Also (g) shows the perturbation due to the self field of the stationary ring.

(3) For the base run, plots of (a) ion ring axial translational energy and (b) theta kinetic energy against time. Plot (c) shows v_z^4 against the axial position (Z) of the ring.

(4) (a) Plot of z_s against $\log(v_{z0}/v_A)$. The dashed line is the gradient taken from Eq. (46), (b) Plot of $\log(z_s/z_A)$ against v_{z0}/v_A.

(5) Numerical check of the scaling laws indicated by Eq. (76).

(6) Plot of the single-particle average axial velocity against the theta magnetic field strength.

(7) Plots of the magnetic field and particle energy.

(8) Selected ion-ring tracer-particle trajectories in the $r - z$ plane.

(9) The quantity $(v_z/v_{z0})^4$ versus Z for slowing down in the presence of axial and toroidal magnetic fields.

(10) (a) Poloidal magnetic field lines, and (b) contours of theta magnetic field for a spheromak surrounded by current-free magnetic fields.

(11) Contours of the potential H^* for a particle that is injected at $r = 75$ cm. a large distance away from the spheromak ($H^*\,|_{\max} = 0.77$ MeV, $H^*\,|_{\min} = 0$).

(12) Single particle trajectories in the (r, z) plane, in the vicinity of a spheromak. The separatrix of the spheromak is indicated by the broken half circle. The axial point of

injection is $z_i = 70$ cm., and the radial points are r_i = (a) 35, (b) 45, (c) 55, (d) 65, (e) 75, (f) 85, (g) 95, and (h) 105 cm.

(13) Contour plot of the potential H^* for a spheromak with a weak ring ($\zeta = 0.25$) nearly.

(14) The coalescence of a weak ring ($\zeta = 0.25$) with a spheromak: (a) poloidal magnetic field lines, and (b) ring particle position.

(15) Axial cross-section of the potential H^* at the ring radius R_b.

(16) Ring translational velocity divided by the Alfvén speed for (a) (Δ) RUN#1, and ($+$) RUN#2, and (b) ($\times$) RUN#3 ad (∇) RUN#4.

(17) The initial accessible areas in the (r, z) plane for (a) RUN#3, and (b) RUN#4.

Table 1: The measured slowing down length z_S compared with the theoretical estimate z_A for various values of the ratio of the initial translational ring velocity to the Alfvén speed.

RUN #	v_{z0}/v_A	z_A (cm)	z_S (cm)
1	1.0	0.06	6.7
2	2.5	2.30	18.0
3	5.0	36.7	77.0
4	8.0	240.0	257.0
5	10.0	587.0	533.0
6	12.0	1220.0	1024.0
7	14.1	2320.0	1690.0

Table 2: Simulation results showing the power law dependence of ring deceleration on various physical quantities.

Quantity	Theoretical Exponent	Measured Exponent
N_b	1	1.1
B_0	4	4.3
a_r	-1	-1.1
a_z	0	-0.24
v_{z0}	-2	-2.4
n_p	-1	-1.04

Table 3: Summarizing the results of the slowing down runs with an externally imposed theta magnetic field.

RUN	B_θ/B_z	ξ	δE_b	ε %	$kv_A\Delta t$	$kv_A^2\Delta t/\Omega_i$
1	0.0	1.0	1.0	1.0	0.17	0.67
2	0.25	1.22	1.30	10.0	0.19	0.77
3	0.5	1.47	1.83	106.0	0.25	1.00
4	1.0	2.03	2.51	240.0	0.40	1.64
5	−0.25	0.80	0.83	1.5	0.19	0.77
6	−0.5	0.62	0.69	7.8	0.25	1.00
7	−1.0	0.33	0.80	45.0	0.40	1.64

Table 4: A summary of the measured slowing down length compared with the calculated slowing down length for RUNS #1, 2, and 5.

RUN	z_A (cm)	z_S (cm)	α	$\left(1+\frac{8}{5}\Delta\right)$
1	650.0	604.0	1.0	1.0
2	533.0	454.0	0.75	0.82
5	767.0	632.0	1.05	1.18

Table 5: The measured slowing down lengths z_S compared with the calculated value $z_A = 2.29$ cm. Note that z_S is measured by plotting v_z^4 against z and taking the appropriate scale length in accordance with Eq. (44) Also, the quantity $k_z c/\omega_i$ is varied by changing a_{zh} or by altering n_p/m_i while keeping the ratio $n_p m_i$ constant. The last column shows ΔB which is the perturbed theta magnetic field energy divided by the perturbed poloidal magnetic field energy. The ratio v_{z0}/v_A is equal to 2.5 for these runs, and μ is the proton mass.

RUN	a_{zh}	$n_p \times 10^{13}$	$m_i\mu$	$k_z c/\omega_i$	z_S/z_A	ΔB
1	30.0	5.0	1.0	0.67	7.95	0.12
2	30.0	16.0	$\sqrt{10}$	6.7	4.66	0.17
3	7.5	5.0	1.0	26.8	2.10	0.31
4	7.5	16.0	$\sqrt{10}$	134.0	3.23	0.55

Table 6: A summary of important characteristics for the case where a weak ring coalesces with a CT.

RUN	ζ	Z_0	ζ_c/ζ	v_{z0}/v_A	NABS %
1	0.25	150.	0.41	50.0	25.0
2	0.125	175.	1.21	0.0	3.0
3	0.25	120.	0.31	0.5	5.0
4	0.05	120.	1.55	0.5	52.0

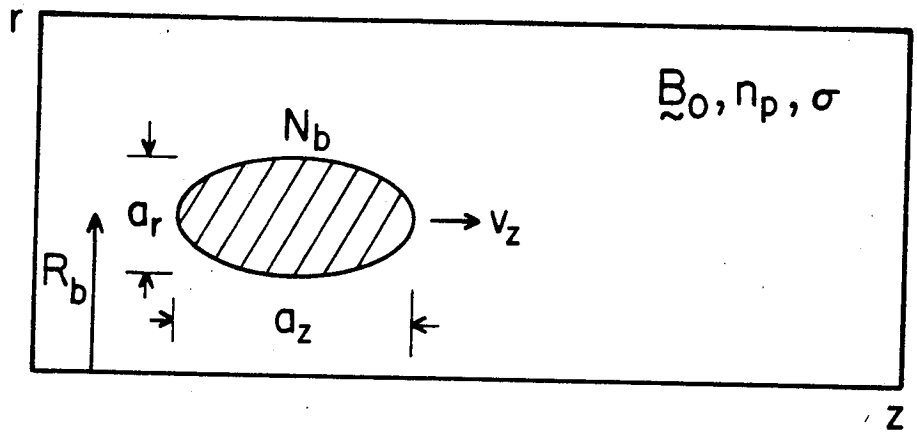

Fig. 1

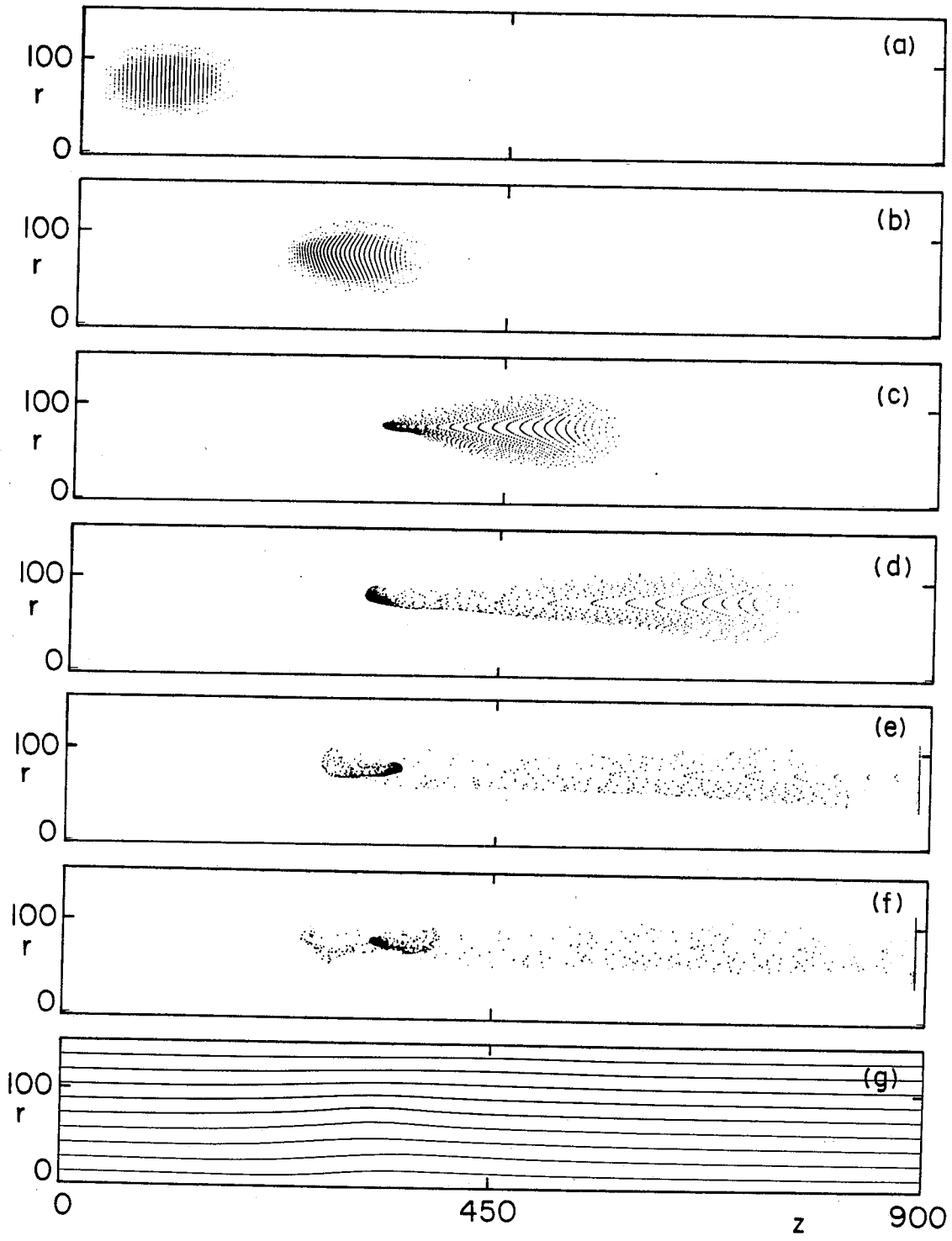

Fig. 2

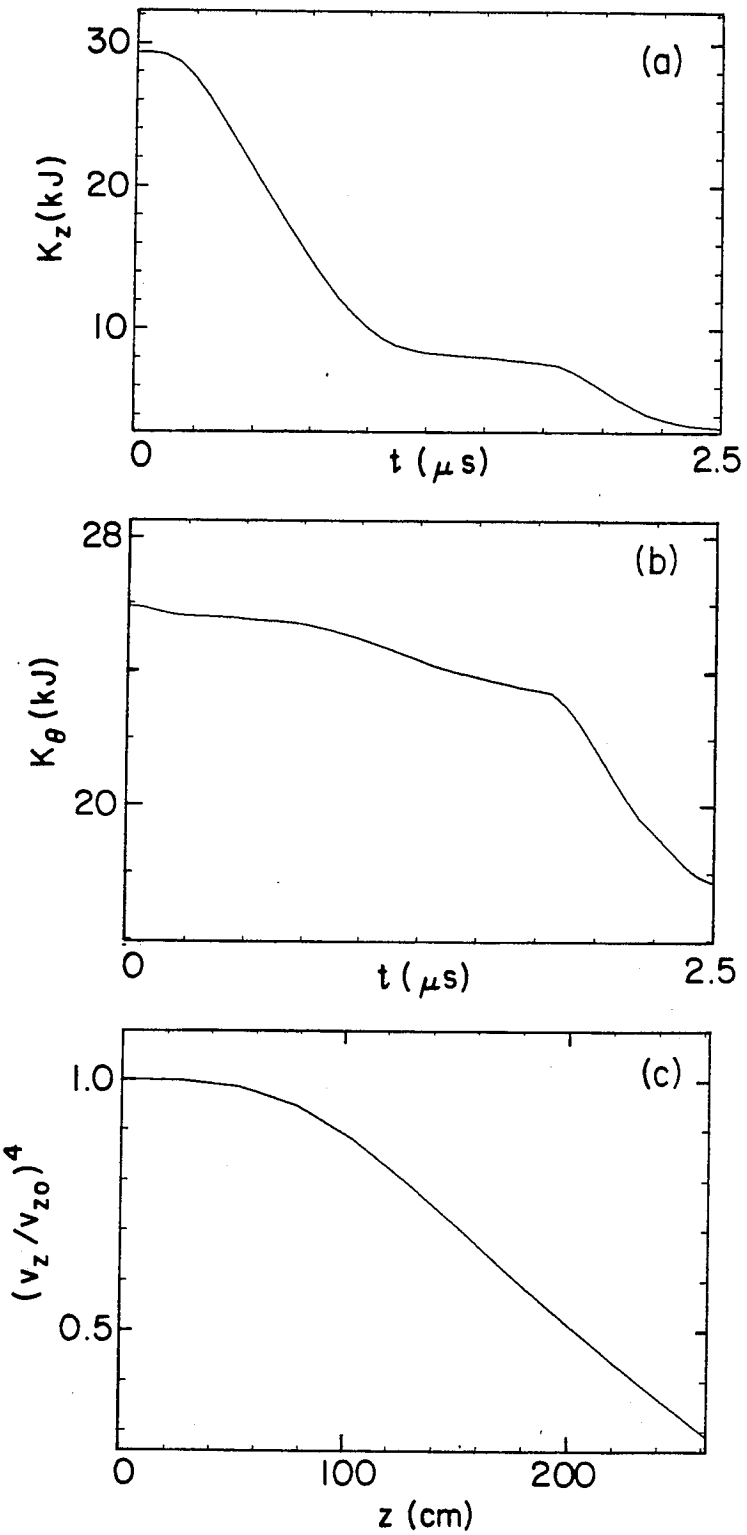
30
20
10
K_z(kJ)
(a)
0
t (μs)
2.5
28
20
K_θ(kJ)
(b)
0
t (μs)
2.5
1.0
0.5
$(v_z/v_{zo})^4$
(c)
0
100
200
z (cm)

Fig. 3

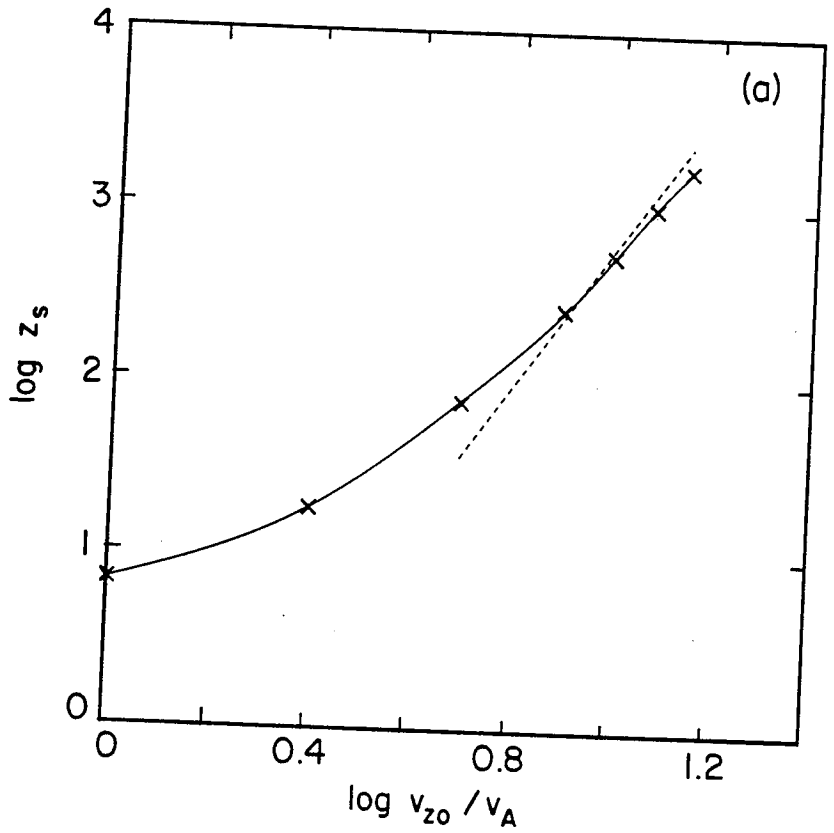

Fig. 4(a)

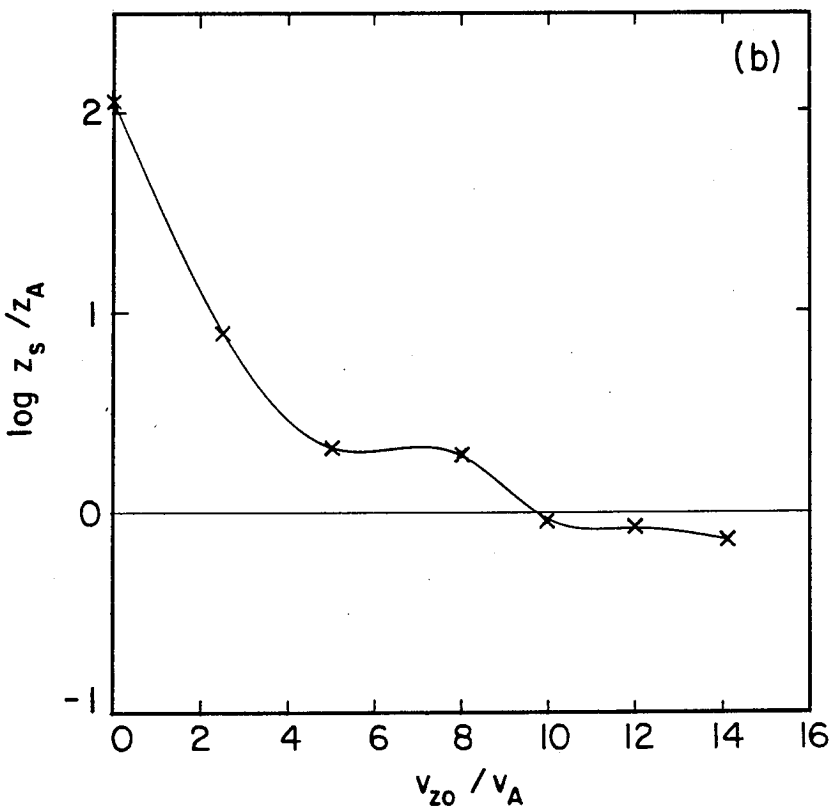

Fig. 4(b)

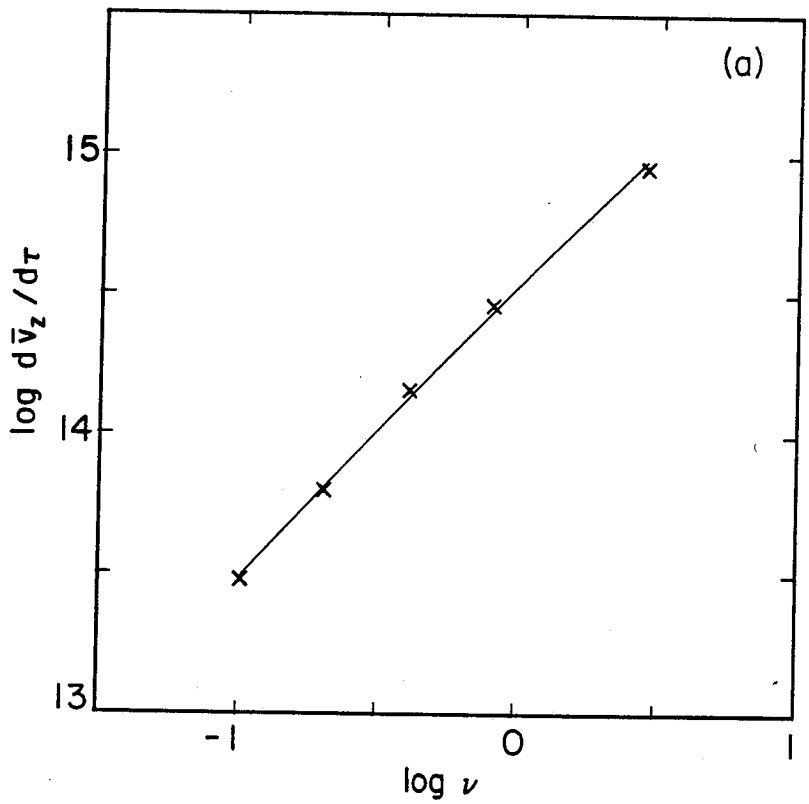

Fig. 5(a)

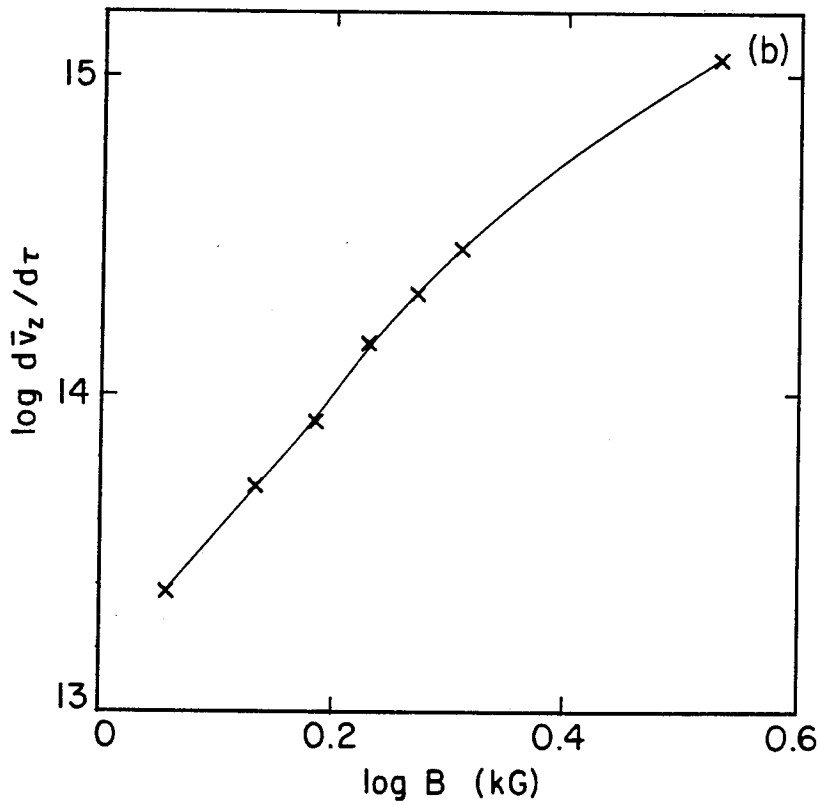

Fig. 5(b)

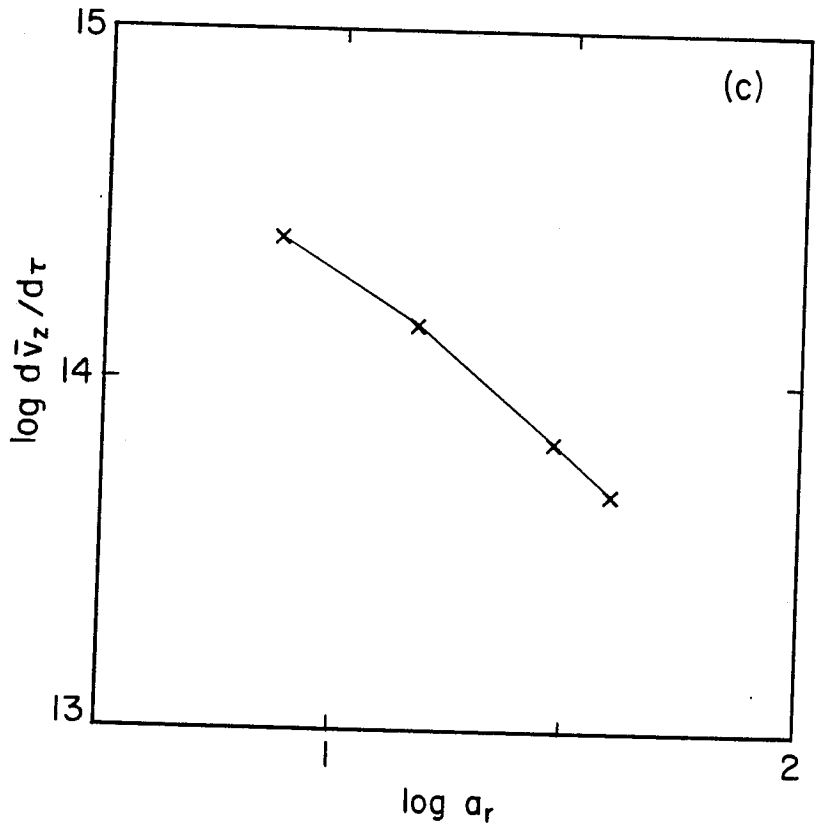

Fig. 5(c)

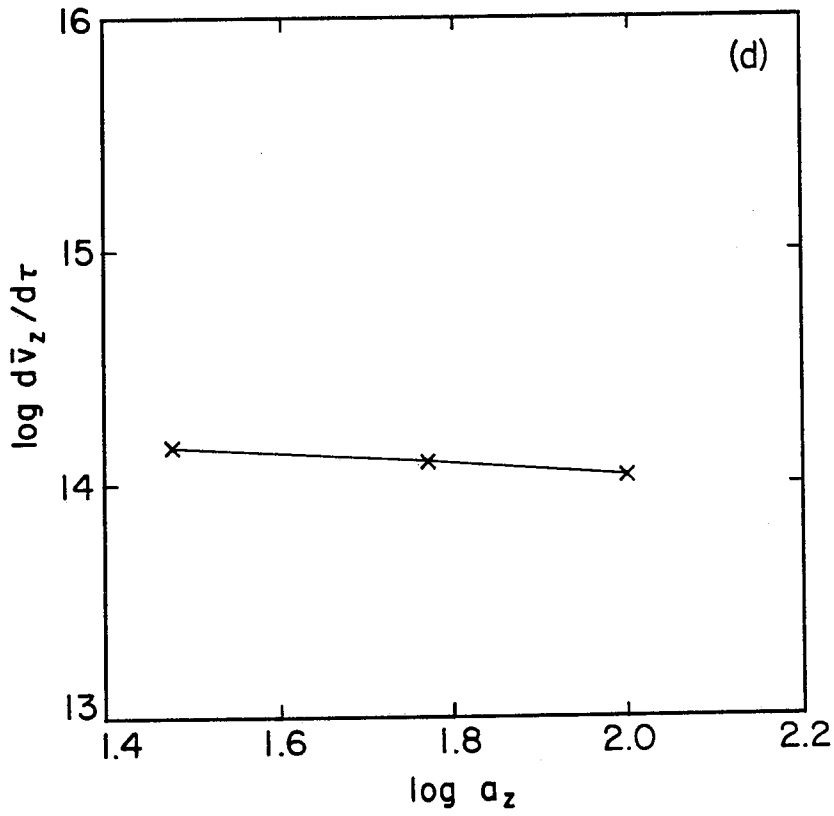

Fig. 5(d)

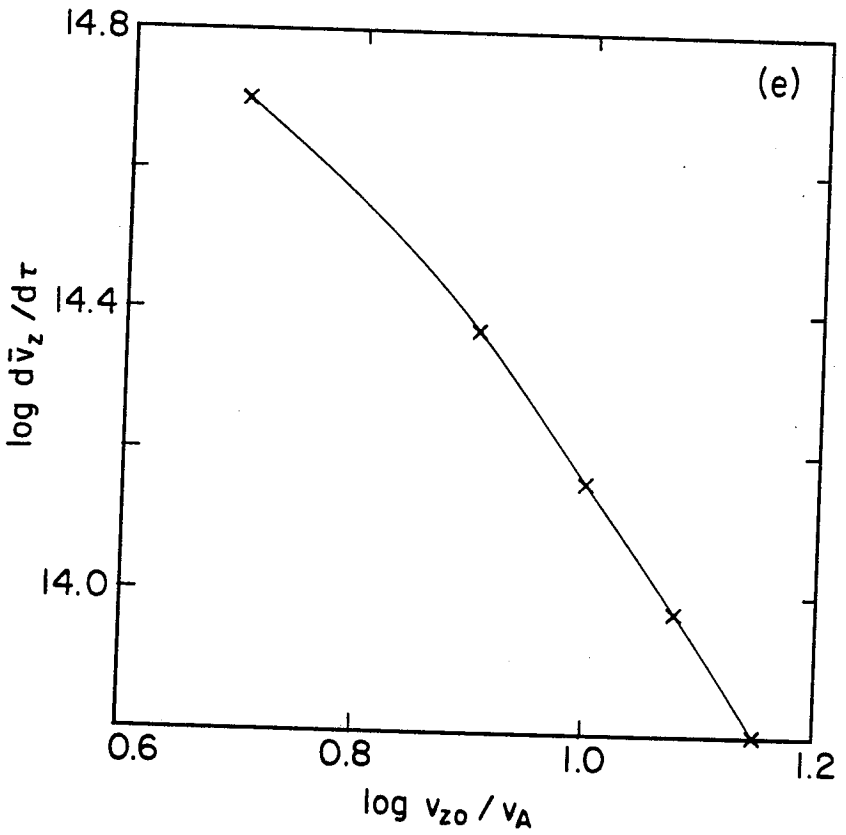

Fig. 5(e)

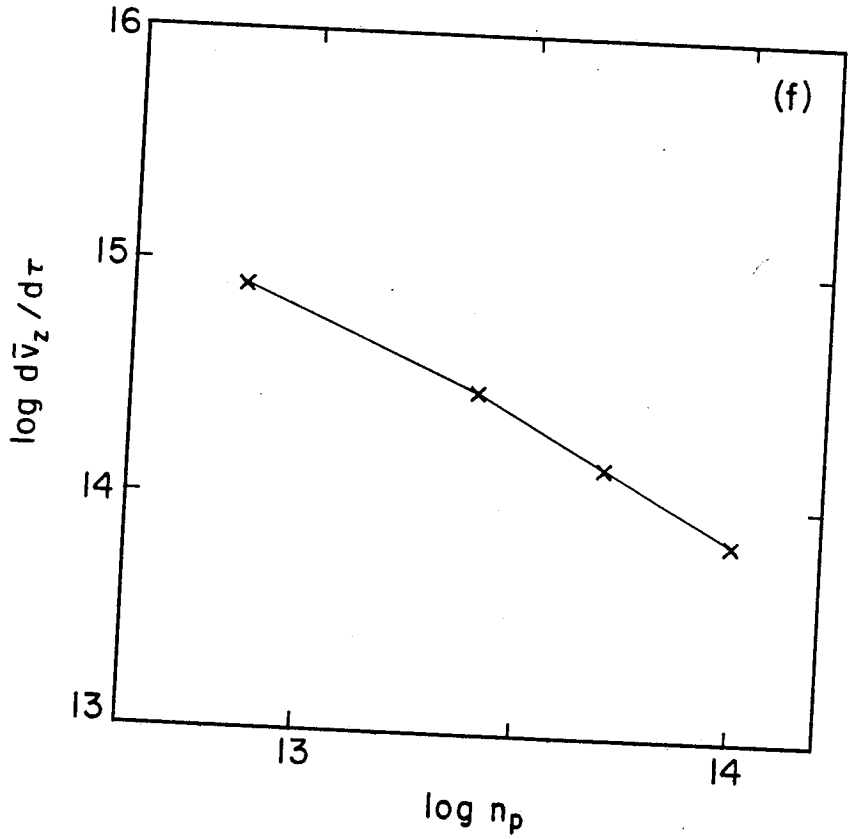

Fig. 5(f)

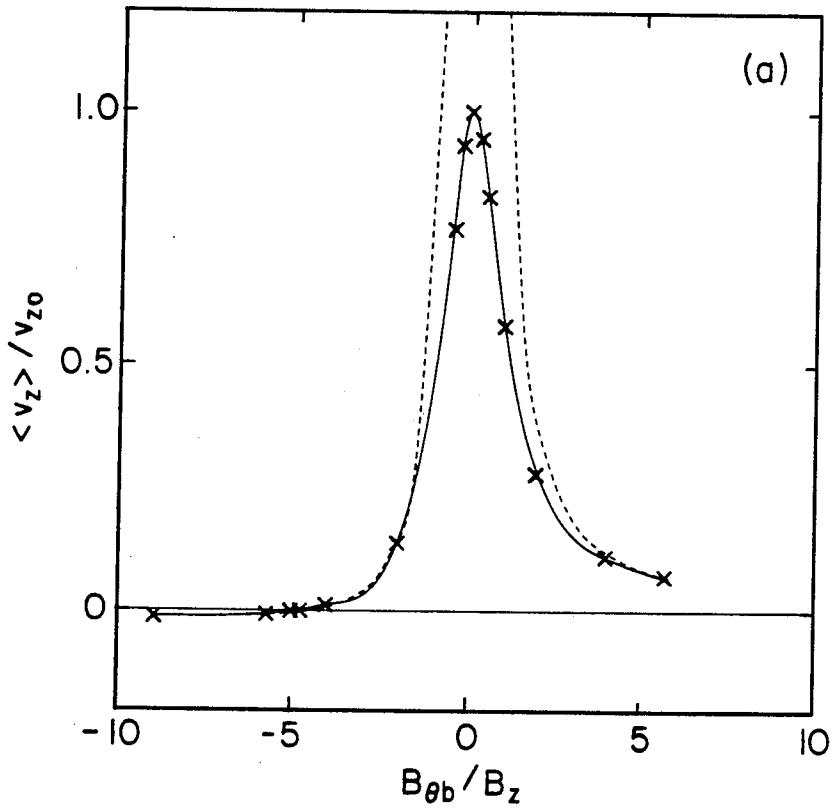

Fig. 6(a)

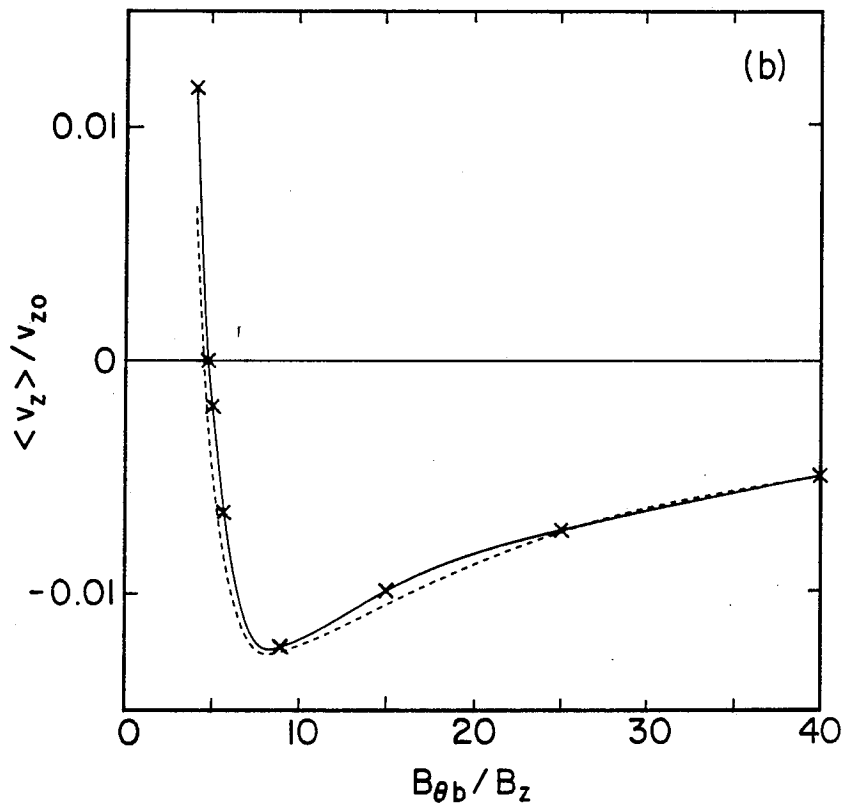

Fig. 6(b)

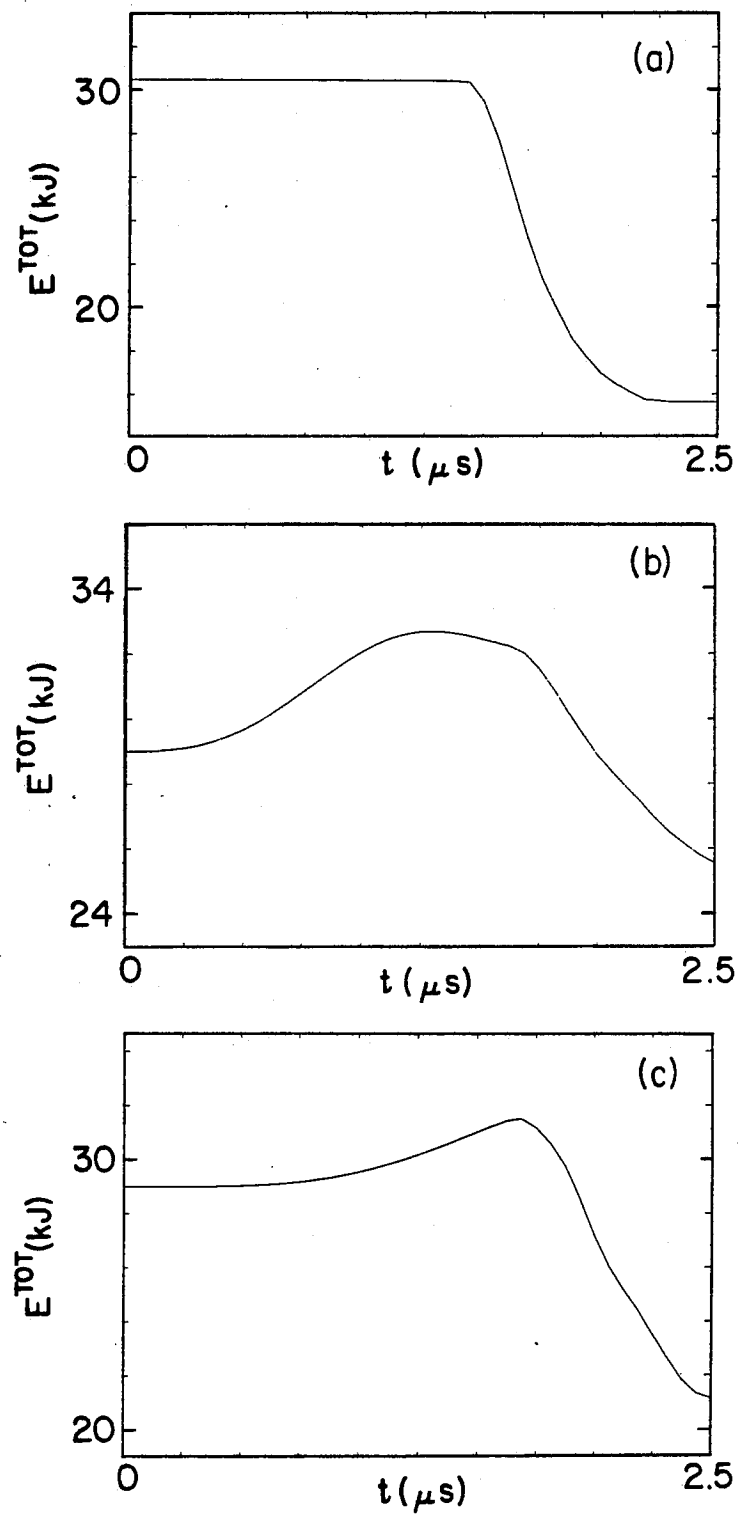
(a)
30
20
E^{TOT}(kJ)
0
t (μs)
2.5
(b)
34
24
E^{TOT}(kJ)
0
t (μs)
2.5
(c)
30
20
E^{TOT}(kJ)
0
t (μs)
2.5

Fig. 7

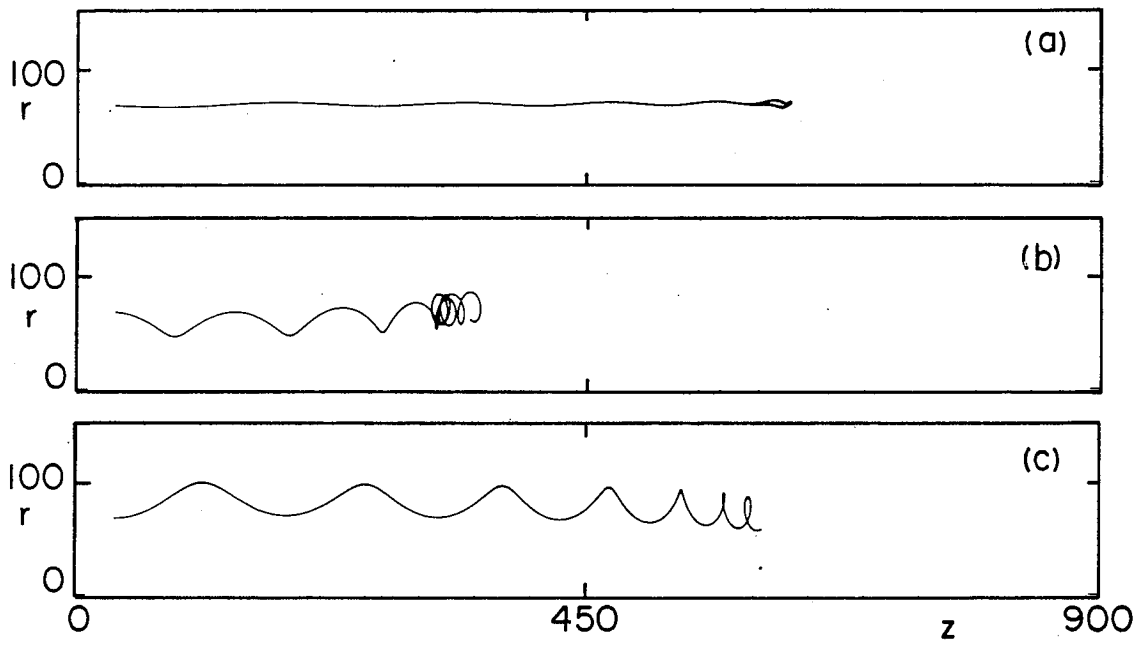

Fig. 8

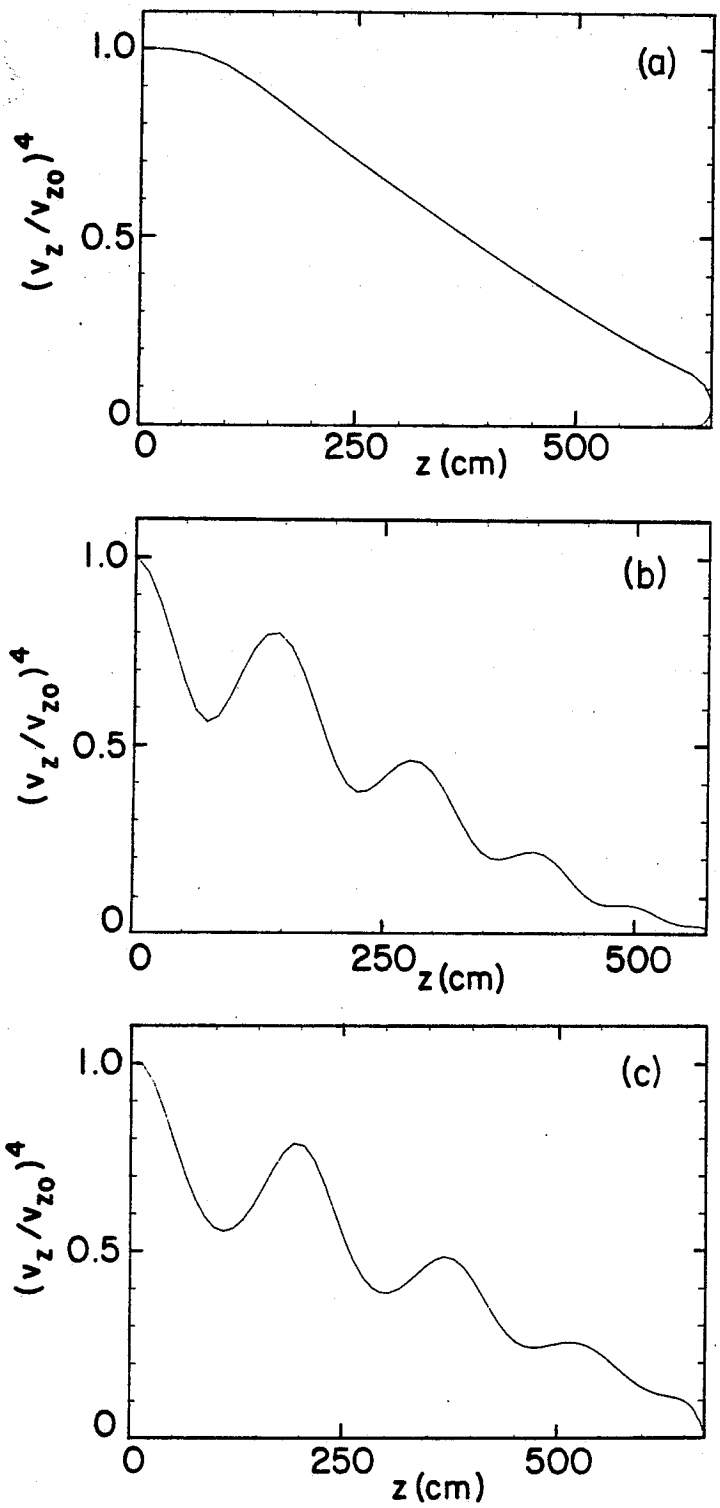

Fig. 9

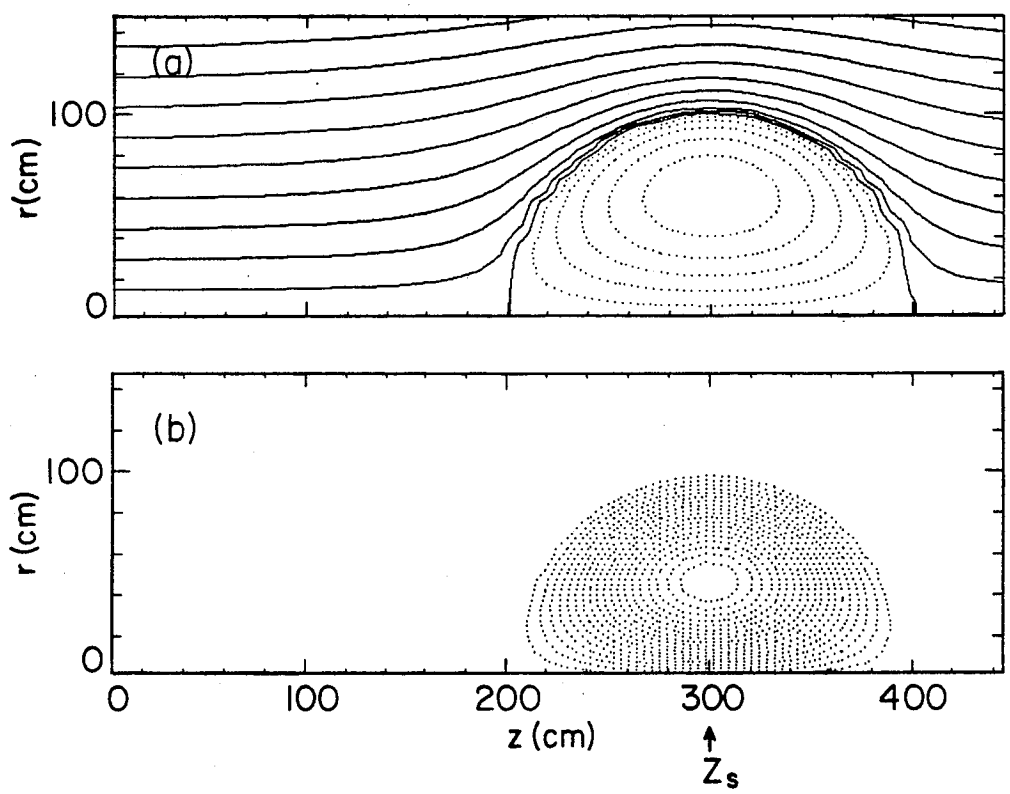

Fig. 10

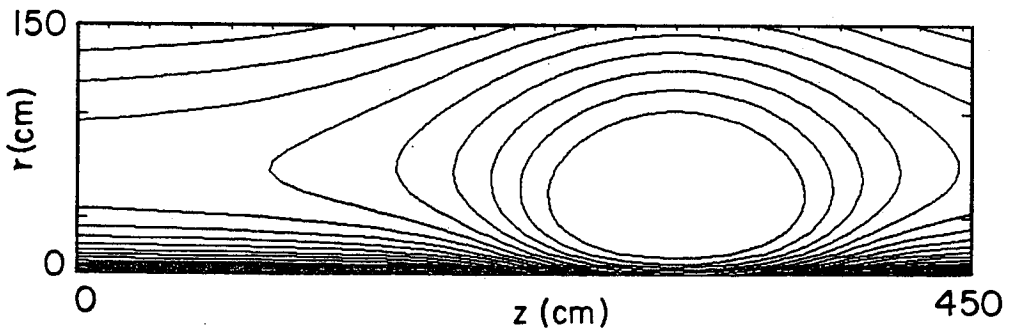

Fig. 11

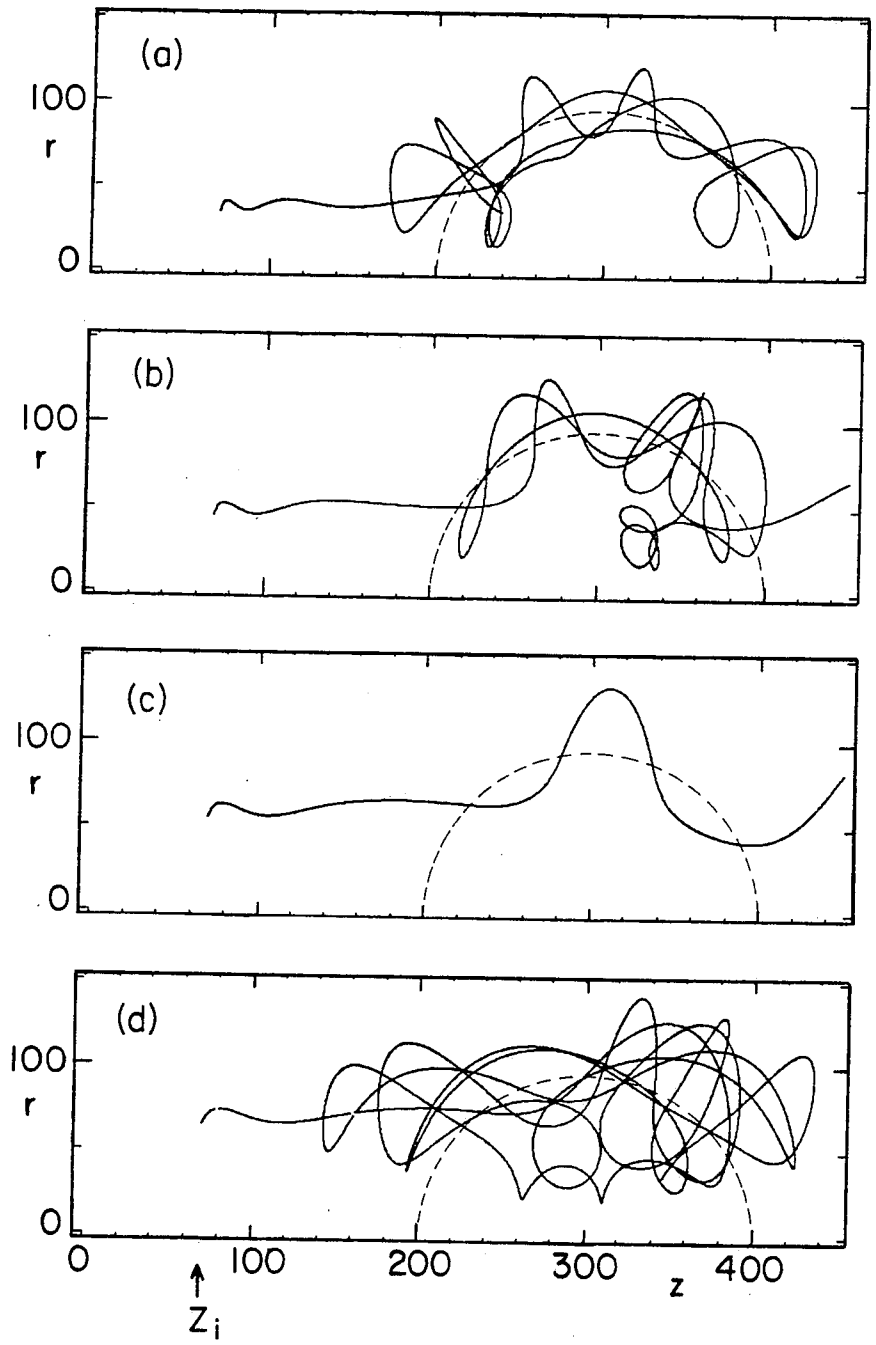

Fig. 12(a)-(d)

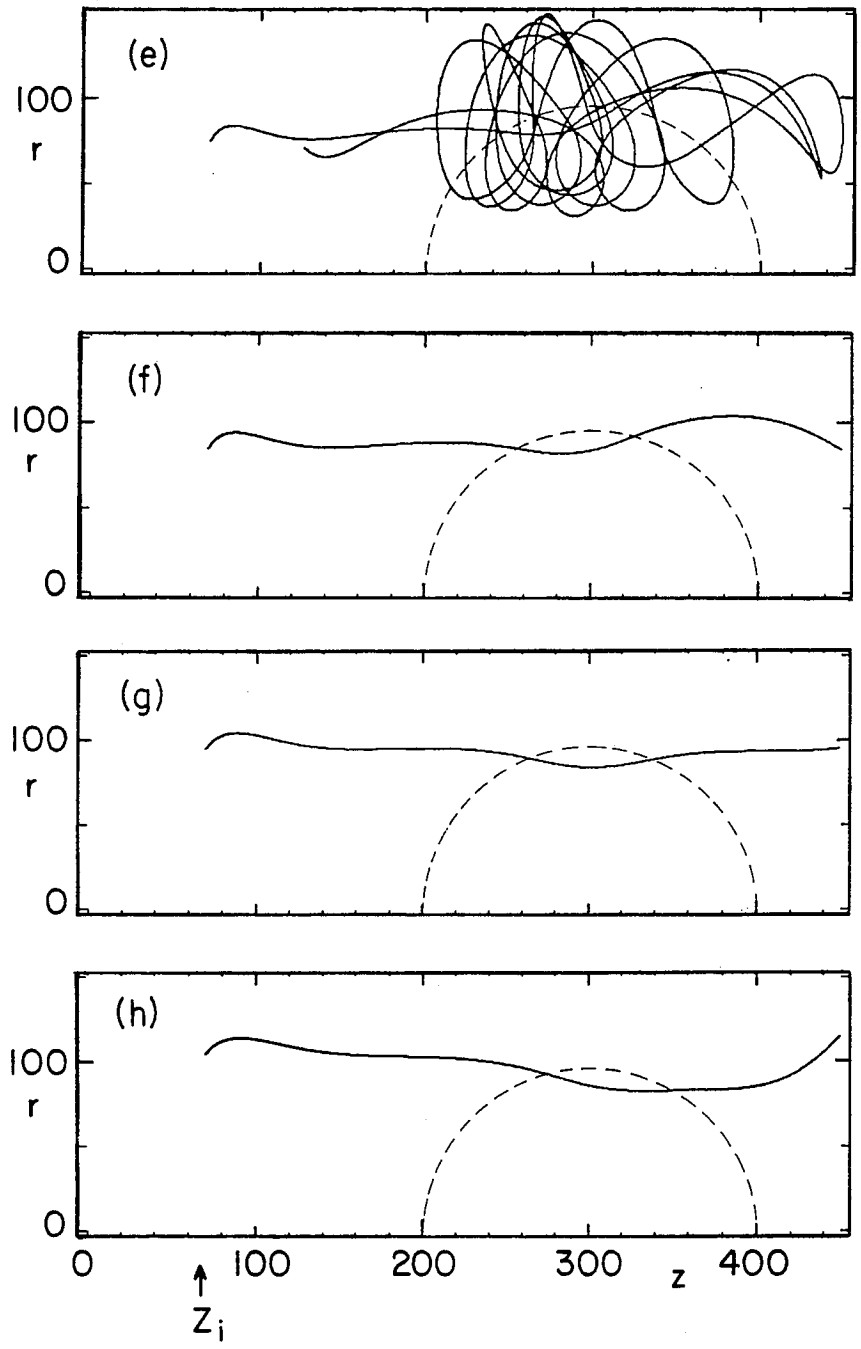

Fig. 12(e)-(h)

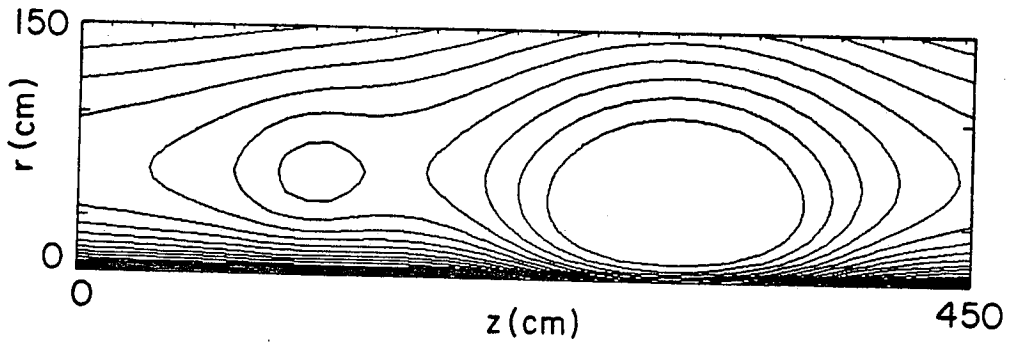

Fig. 13

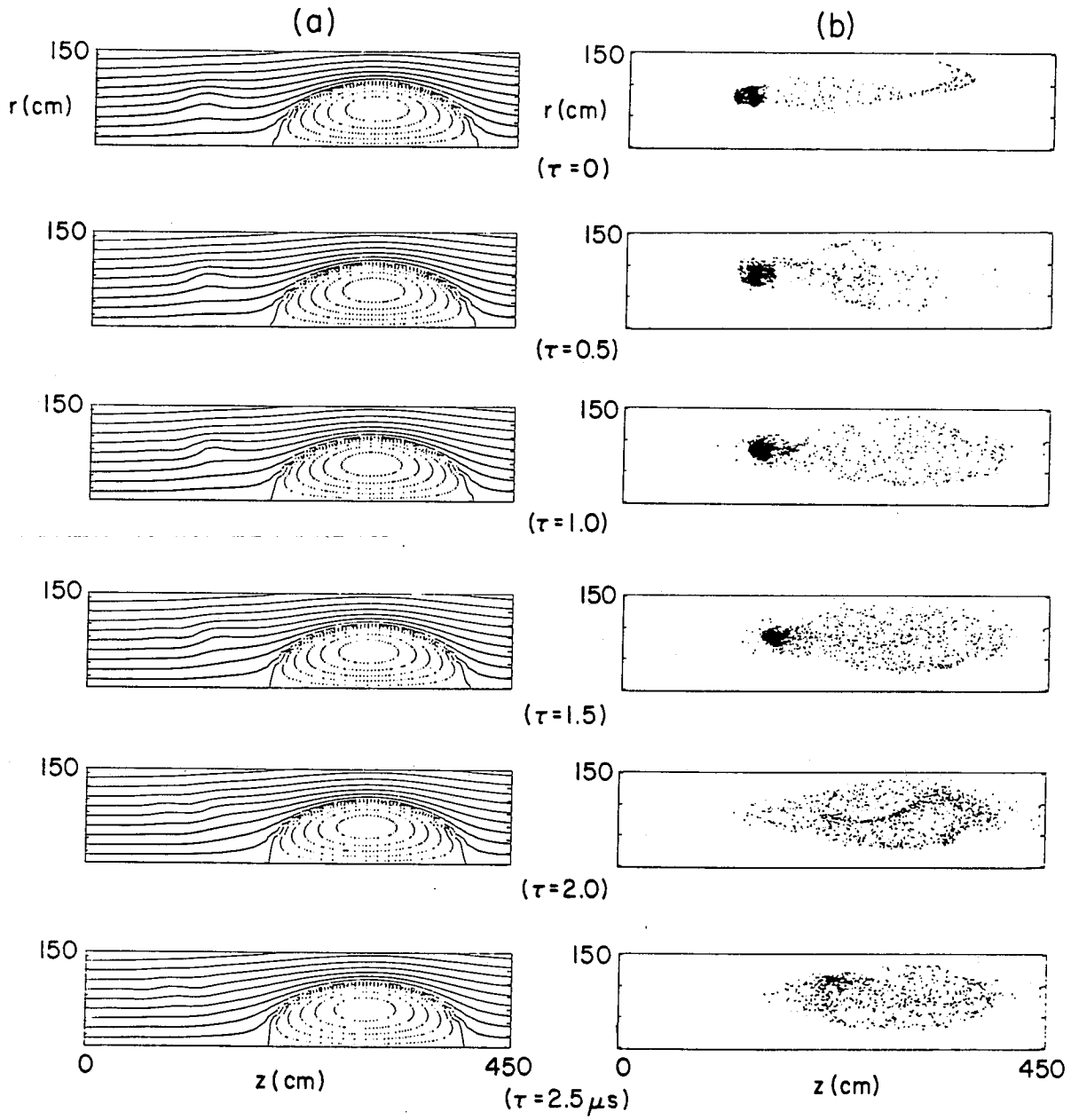

Fig. 14

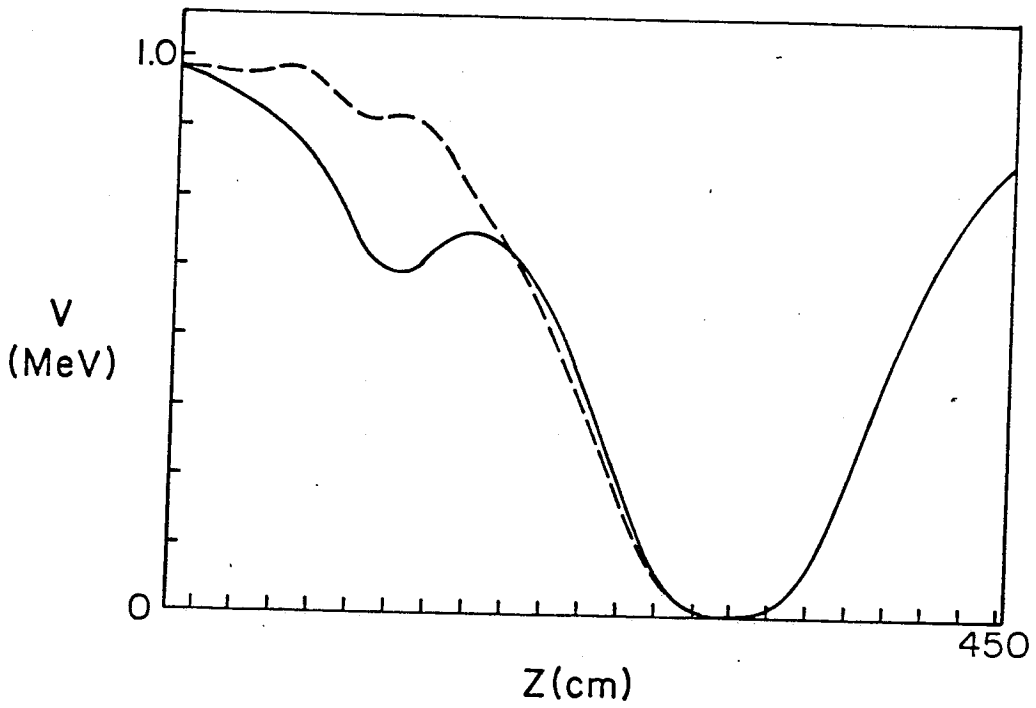

Fig. 15

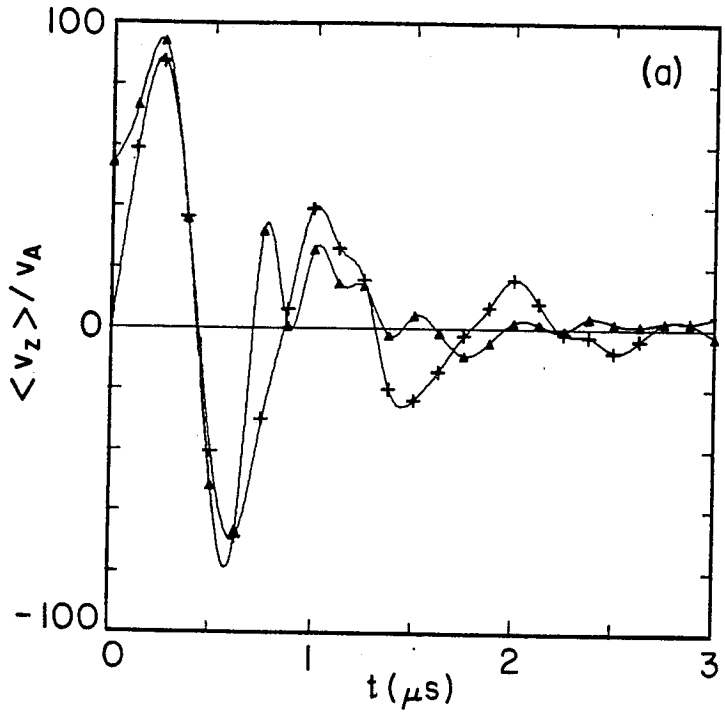

Fig. 16(a)

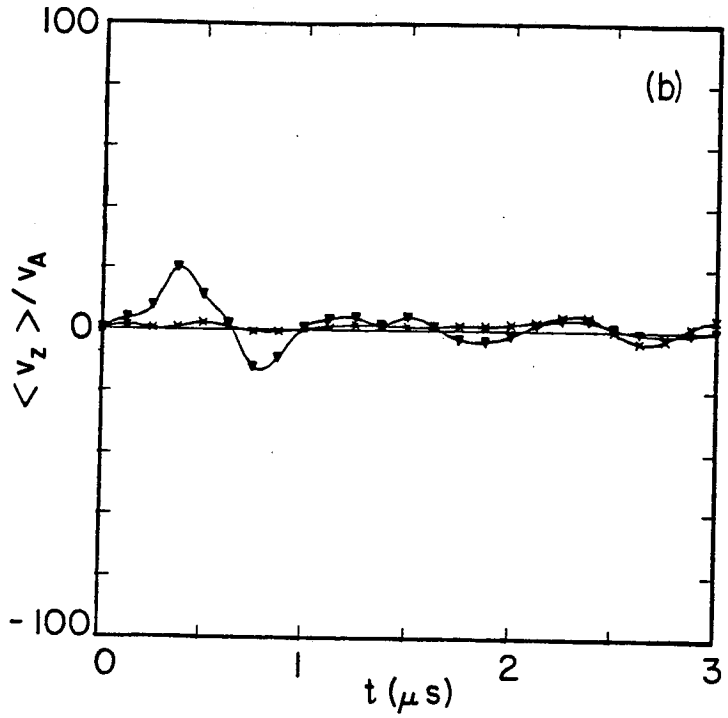

Fig. 16(b)

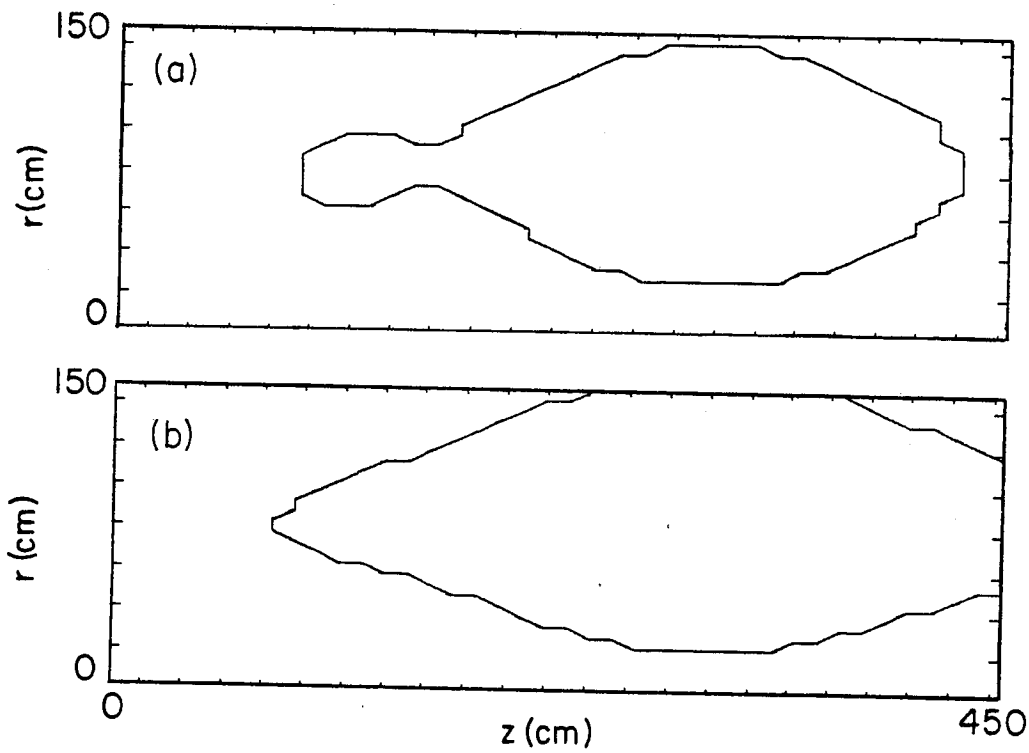

Fig. 17